SHOCK MITIGATION WITH LIGHTWEIGHT VERMICULITE CONCRETE

by Richard Shield, Ervin S. Perry, E. A. Ripperger, and J. Neils Thompson

February 1962

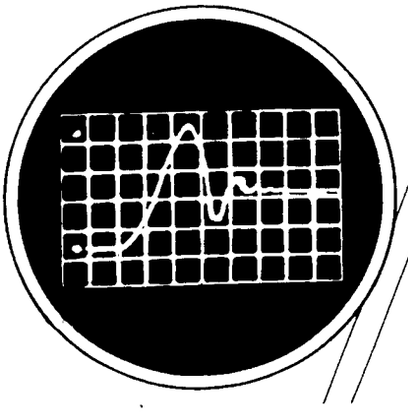

STRUCTURAL MECHANICS RESEARCH LABORATORY
THE UNIVERSITY OF TEXAS
BALCONES RESEARCH CENTER
AUSTIN, TEXAS

DASA 1263

UNCLASSIFIED

SHOCK MITIGATION WITH LIGHTWEIGHT VERMICULITE CONCRETE

by

Richard Shield
Ervin S. Perry
E. A. Ripperger
J. Neils Thompson

Prepared for

DEFENSE ATOMIC SUPPORT AGENCY

Contract DA 49-146-XZ-028

Nuclear Weapons Effect Research Subtask 13.040

THE UNIVERSITY OF TEXAS

STRUCTURAL MECHANICS RESEARCH LABORATORY

Austin, Texas

February 1962

The Structural Mechanics Research Laboratory

is cooperatively operated by

The Engineering Mechanics and Civil Engineering Departments

at

The Balcones Research Center

University of Texas

Austin, Texas

PREFACE

The behavior of underground structures that have been subjected to blast-type loadings has indicated that if crushable-type material is used as a backfill, the structure will be subjected to reduced accelerations. This report is the second in a series to explore the potential of high-air-content, lightweight concrete with low-strength aggregate as a shock mitigator or shock isolator.

Because of the nature of the type of material, it was considered necessary to investigate the effect of the rate of deformation on the stress-strain characteristics. This investigation is a continuation of a previous study of lightweight concrete using vermiculite aggregate. In the early study, deformation rates up to 60 ft per second were employed. In this investigation, a different technique and deformation rates up to 120 ft per second were studied.

Directing Staff:

J. Neils Thompson, Director of Structural Mechanics Research Laboratory, Professor of Civil Engineering Department

E. A. Ripperger, Associate Director of Structural Mechanics Research Laboratory, Professor of Engineering Mechanics Department

Richard Shield, Research Engineer I

Ervin Perry, Research Engineer II

Clarke Covington, Research Engineer I

Eugene Smith, Research Engineer (Faculty)

J. Neils Thompson
Director
Structural Mechanics Research Laboratory
The University of Texas
Austin, Texas

March 1962

TABLE OF CONTENTS

TABLE OF CONTENTS
(Cont'd)

TABLE OF CONTENTS
(Cont'd)

LIST OF FIGURES

LIST OF FIGURES
(Cont'd)

ABSTRACT

The impact cushioning characteristics of lightweight vermiculite concrete are presented in the form of acceleration-time and stress-strain curves. Data are included which show the effect of impact velocity and material thickness on the cushioning properties.

The measurement technique used is a variation of the one used at the drop-test facility for the determination of the properties of cushioning materials, the essential difference being that the force-sensing device, an accelerometer, is allowed to move. Also, impact energy is provided by a projectile fired from an air gun, instead of a freely falling mass.

INTRODUCTION

In a report, Isolation of Structures from Ground Shock,[1*] by Stanford Research Institute, the final results are described of one of the 46 projects comprising the military-effect program of Operation Plumbbob, which included 24 test detonations at the Nevada Test Site in 1957.

The Nevada test project was a study of the benefit of frangible backfill in isolating or protecting underground structures from violent motions produced by explosions in their vicinity. Acceleration measurements were made on two test structures and one comparison structure. Each test structure consisted of a reinforced concrete pipe enclosing a steel cylinder separated from the pipe by "O"-rings. The two test structures were isolated from the surrounding soil with a lining of frangible backfill (glass bottles) around the sides and bottom. The comparison structure consisted only of a concrete pipe with a solid concrete bottom. The measured peak accelerations produced by normal and shear forces in the two isolated structures were significantly lower than those measured in the structure with no barrier. Since the comparison structure contained no steel cylinder and "O"-rings, the data from the two systems could not be directly correlated. It was felt, however, that the lower respective accelerations in the isolated structures were due in part to the crushable backfill. It was concluded that some form of isolating material would be beneficial in reducing the shock sustained by a buried structure under the influence of a blast wave.

---

*Numbers indicate references as listed in Bibliography.

A fairly complete summary of the areas worthy of investigation in this field is given in the Recommendations section of the Stanford report.[1] These recommendations are included here to help explain the nature of the problem and the objective of the present investigation.

The general recommendation is that theoretical, laboratory, and field-test studies of the merit of special backfills should be undertaken. These studies should include investigation of a variety of backfills and the determination of (1) their properties as shear and as compression barriers, (2) their permeability to water, (3) their tendency to creep, (4) their placement problems, and (5) their cost.

Specifically, it is recommended that:

1. Laboratory tests be performed to determine the appropriate properties of promising materials. The properties should include compressive stress-strain characteristics under both static and dynamic conditions, and, if possible, shear properties under dynamic inputs. The materials should include foamed materials (plastic and cement concrete) and frangible materials.

2. Analytical studies be undertaken to outline the range of properties desired and to obtain some indication of the relative importance or value of each. This phase should probably include some specific examples. It might well include some consideration of the probabilities of repeated attack to permit an evaluation of the relative value of multi-shot protection versus single-shot protection.

3. Field tests be performed to establish the capability of appropriate materials as compression barriers. Megaton tests are important for this purpose because the long duration of high pressure is difficult for compression barriers to withstand.

A test with kiloton devices will almost surely be successful, but this may result in misleading extrapolation to megaton inputs.

4. Field tests be performed to determine the shear capabilities of additional materials and configurations. These tests might well include those of the capabilities against more than one attack. Megaton inputs are to be preferred as being more definitive, but kiloton tests would be of value.

On March 1, 1960, the Defense Atomic Support Agency contracted with The University of Texas (Structural Mechanics Research Laboratory) to make a feasibility and an experimental study of materials and systems for the isolation of underground structures subjected to dynamic loads.

Under this contract, an experimental investigation was initiated to study the stress-strain properties and impact cushioning characteristics of lightweight concrete. After a preliminary study of various aggregate materials including vermiculite, perlite, pumice, and cinders, it was decided that among these, vermiculite concrete exhibited the most promising properties as a backfill for cushioning underground structures.

The investigation was conducted in two separate, but closely coordinated, phases. One phase included the study of stress-strain and stress-time curves produced by impacting confined vermiculite concrete on a fixed force-plate dynamometer with a freely falling mass. The work was performed by Covington[2] at the 275-ft drop tower located at Balcones Research Center.

The scope of that portion of the investigation included variation of impact velocity from 10 to 60 fps, and variation of impacting mass from 236 to 611 pounds. All of the impact drops were made with constant input-energy-per-unit volume of material.

The second phase of the investigation, which is described in this report, includes a series of high-velocity impacts on confined vermiculite concrete.

The measurement technique used is a variation of the one used at the drop-test facility for determination of the properties of cushioning material, the essential difference being that the force-sensing device, an accelerometer, is allowed to move. Also, impact energy is provided by a projectile fired from an air gun, instead of a freely falling mass.

Tapley[3] has shown that the oscillations in stress-time and stress-strain curves obtained by the fixed force-plate and falling mass technique may be attributed to the natural frequency of oscillation of the dynamometer system. The peaks of these oscillations are usually smoothed out and neglected in the presentation of stress-strain and stress-time records. The energy absorption represented by a smooth curve drawn through the oscillations in the dynamometer record has been found to correspond closely to the available energy of impact, probably because the areas under the smooth curve and the actual curve do not differ appreciably. Since energy dissipation of materials has been of primary concern in the past, this technique has been satisfactory when one material was to be compared with another.

However, since some of the peaks in the actual stress-time records

may be as much as 50 per cent higher than the average crushing stress, it is essential that it be determined if these peaks have any significant effect on the acceleration transmitted through a cushion to a cushioned mass. Also, it has been shown recently by several investigations [4, 5, 6, 7] that the ratio of rise time of an impulse to the natural period of a cushioned system is a significant factor in determining the response of the system. In other words, the deflection or permanent deformation of a cushioned structure may be very dependent upon the shape and duration of the shock impulse and on the rise time of the initial peak.

Finally, it should be noted that the drop-tower facility provides a maximum impact velocity of approximately 110 fps. At that velocity, with the smallest impact mass usually used, 236 lb, a very large volume (about 2.5 ft^3) of cushioning material is required. With the air gun used in the acceleration studies, impact velocities as high as 500 fps are readily attainable, and a large volume of cushioning material is not required. Also, it is possible to obtain stress-strain curves by double integration of the acceleration-time record for the accelerated mass and projectile respectively. Although this procedure (see Experimental Program) involves considerable calculation and replotting, or solution by a computer, it serves as a good check on the reliability of the data taken with the accelerometer.

In view of the above comments, it seems reasonable that if a correlation between the two methods can be established, it will greatly facilitate the gathering of data concerning materials.

EXPERIMENTAL PROGRAM

Scope

Measurements were made to determine the effectiveness of light-weight vermiculite concrete in reducing the magnitude of the acceleration imparted to a mass by another impacting mass. Impact acceleration records were made by using a compressed air gun firing a 4-in. -diameter, 25-lb steel projectile at an assembly consisting of a 98-lb mass cushioned with a laterally confined cylinder of concrete. Fig. 1 shows an over-all view of the apparatus.

Two series of acceleration-time measurements were made with the 4-in. -bore air gun. They were:

(1) Variation in impact velocity from 24 to 120 fps

(2) Variation in thickness of cushioning material from 2 to 4 inches.

Description of Materials

Vermiculite. Vermiculite is a micaceous mineral that exfoliates when heated to form a highly porous, low-density aggregate. The vermiculite used in this investigation is identified as Zonolite Plaster Aggregate No. 3, sold commercially by the Texas Vermiculite Corporation of Dallas, Texas. The No. 3 vermiculite aggregate has a density of 7 to 10 lb per cu ft, and is sized so that virtually all of the material passes a No. 8 sieve; and all of it is retained on a No. 50 sieve.[2]

Cement. Type 1 Portland cement, made by the Alamo Cement Company,

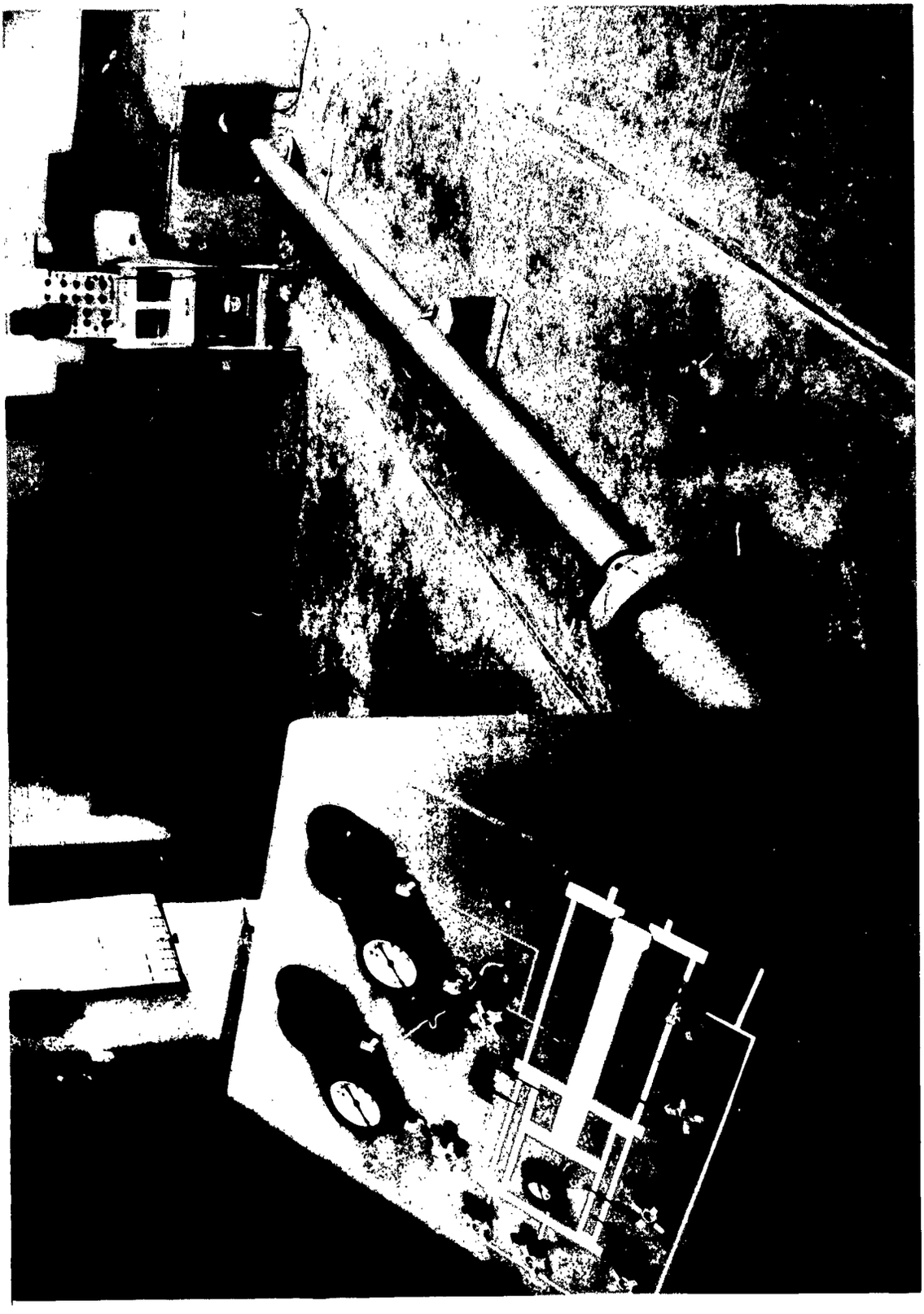

Fig. 1. Four-In.-Bore Air Gun.

San Antonio, Texas, was used in the preparation of the concrete. The density of Portland cement is 94 lb per cubic foot.

Admixture. A neutralized vinsol resin made by the Hercules Powder Company was used as an air-entraining agent, and to produce a more plastic mix. An admixture of this type generally is used when lightweight concrete is pumped into place because less power is required for a given water content, and there is less tendency for the cement to settle out of the mixture.

Preparation of Specimens

Mixing. The concrete investigated was mixed with the following composition per batch:

Expanded vermiculite aggregate	-	2 cu ft
Portland cement	-	0.25 cu ft
Water	-	0.77 cu ft
Admixture	-	100 gm

This mix gave a cement-to-aggregate ratio of one-to-eight by volume. A one to eight mix was chosen because the preliminary study showed that vermiculite concrete mixed in this ratio had a crushing stress within the range requested by the Defense Atomic Support Agency. Also, any greater cement-to-aggregate ratio would have required a larger amount of material for cushioning than was practical with the test apparatus, particularly at the higher velocity levels and consequent higher energy levels.

Water content of the mix was chosen to give a consistency suitable for pumping. After this amount of water was determined, it was held constant in the preparation of all batches. The measured slump with this amount of water was approximately 8 inches.

The amount of air entrained in the mix with the admixture was measured with a Washington Air-Testing Meter, and was measured to be greater than the maximum meter reading of 20 per cent. An extrapolation of the meter scale gave a reading of between 25 and 30 per cent. The air meter measured 8 per-cent air content in a special mix with no admixture because of the porous aggregate, so the actual air entrainment due to the admixture was somewhat less than that measured.

Although a special effort was made to control the uniformity of the concrete mix, the density varied between 47 and 53 lb/ft^3 from batch to batch. However, in this investigation, the specimens were selected to maintain a density variation between 50 and 53 lb per cubic foot.

Curing. Specimens were poured and cured for 2 days in standard 6 by 12-in. steel cylindrical forms. After removal from the forms, the specimens were cured for at least 28 days in a 100 per-cent-humidity room, or in sealed plastic bags. Some of the specimens may be seen in their sealed bags at the top of Fig. 2. Specimens were sawed to required testing length immediately before use, and their faces were scraped until plane.

Instrumentation

Air gun and projectile. A 4-in. -bore compressed air gun capable of firing projectiles with a maximum energy of 1.3×10^5 ft -lb was used to provide a means for varying the impact energy imparted to the cushioning specimens. The gun was designed by Sandia Corporation of Albuquerque, New Mexico, and built by the Structural Mechanics Research Laboratory for high-velocity impact studies. Basically, the gun consists of a pressure-firing chamber

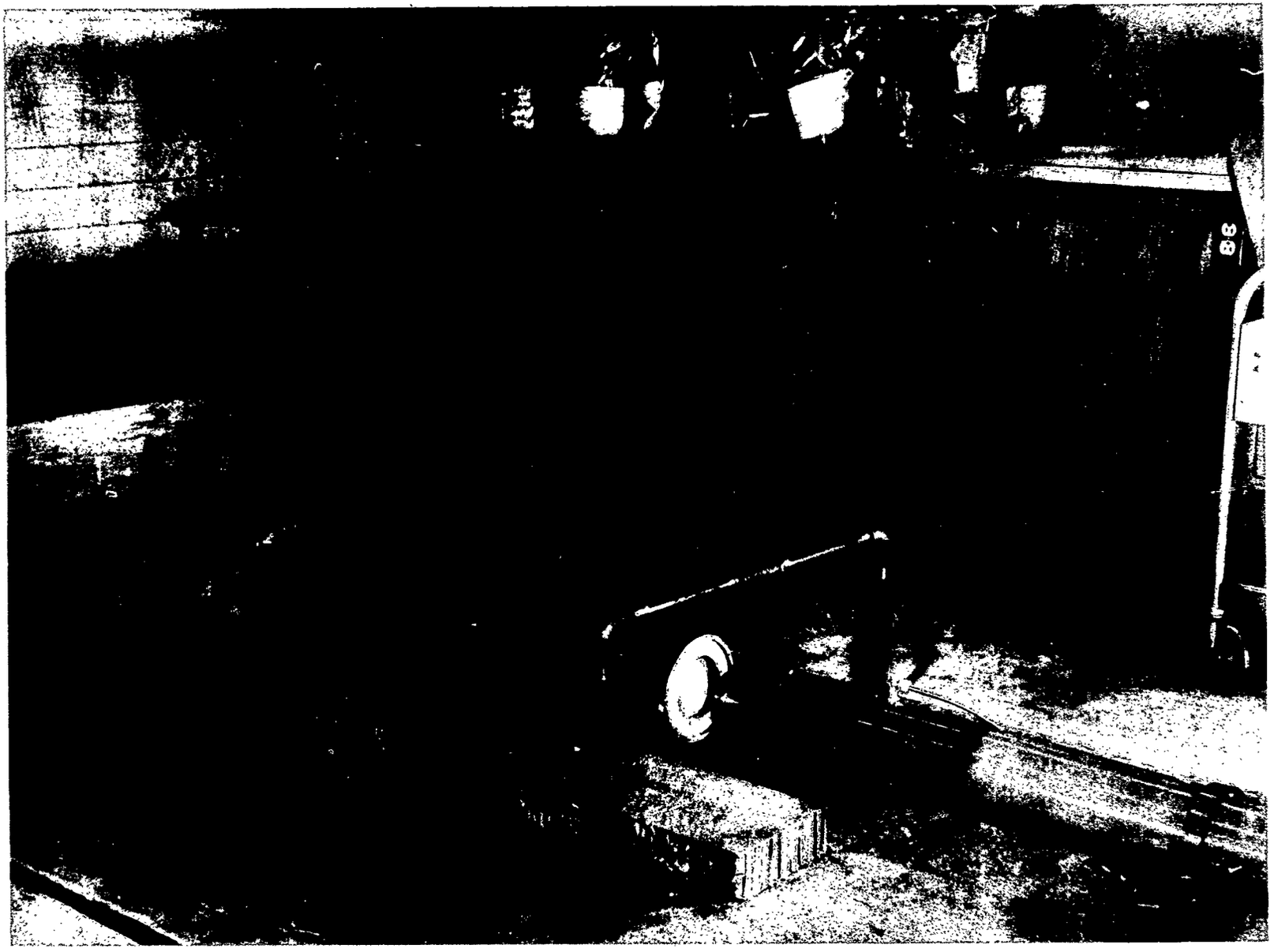

Fig. 2. Acceleration Apparatus for High-Velocity Impact Studies on Confined Vermiculite Concrete.

from which pressure is released abruptly into a barrel by means of a fast-action, accumulator-piston arrangement. Four separate air-pressure chambers are used to fire the projectile at a desired velocity (see Fig. 3). When chamber A is pressurized to a pressure P_a, the valve piston moves forward and seats the valve plug that is attached to the valve piston rod. The valve plug is shown in its seated position. The projectile is muzzle-loaded, and, by capping the muzzle and introducing compressed air into the barrel, the projectile is seated just forward of the valve plug that separates chamber B from the barrel. Chamber B is then pressurized to whatever pressure is necessary for the velocity desired, and chamber C is raised to a pressure somewhat greater than Chamber A. To fire the projectile, the compressed air in chamber C is admitted into chamber D through a quick-release valve. The high pressure in chamber D causes the valve piston to move against P_a, unseating the valve plug and thereby opening chamber B to the barrel. The expanding air from chamber B propels the projectile down the barrel and into the impact specimen.

A 7-in. -long, 25-lb projectile made of mild steel was used for a projectile throughout the series of shots.

Specimen assembly and support. An assembly was made to support the system to be accelerated which would provide minimum friction during impact. The acceleration mass, confined concrete, and accelerometer were suspended by two short, right-angle hooks from a simple pipe frame, in front of the gun, and carefully aligned to provide a plane impact. The cushioning sample was confined in a 20-lb, 6-in. -diameter pipe which was bolted to an acceleration mass, thereby giving a rigid single-mass system.

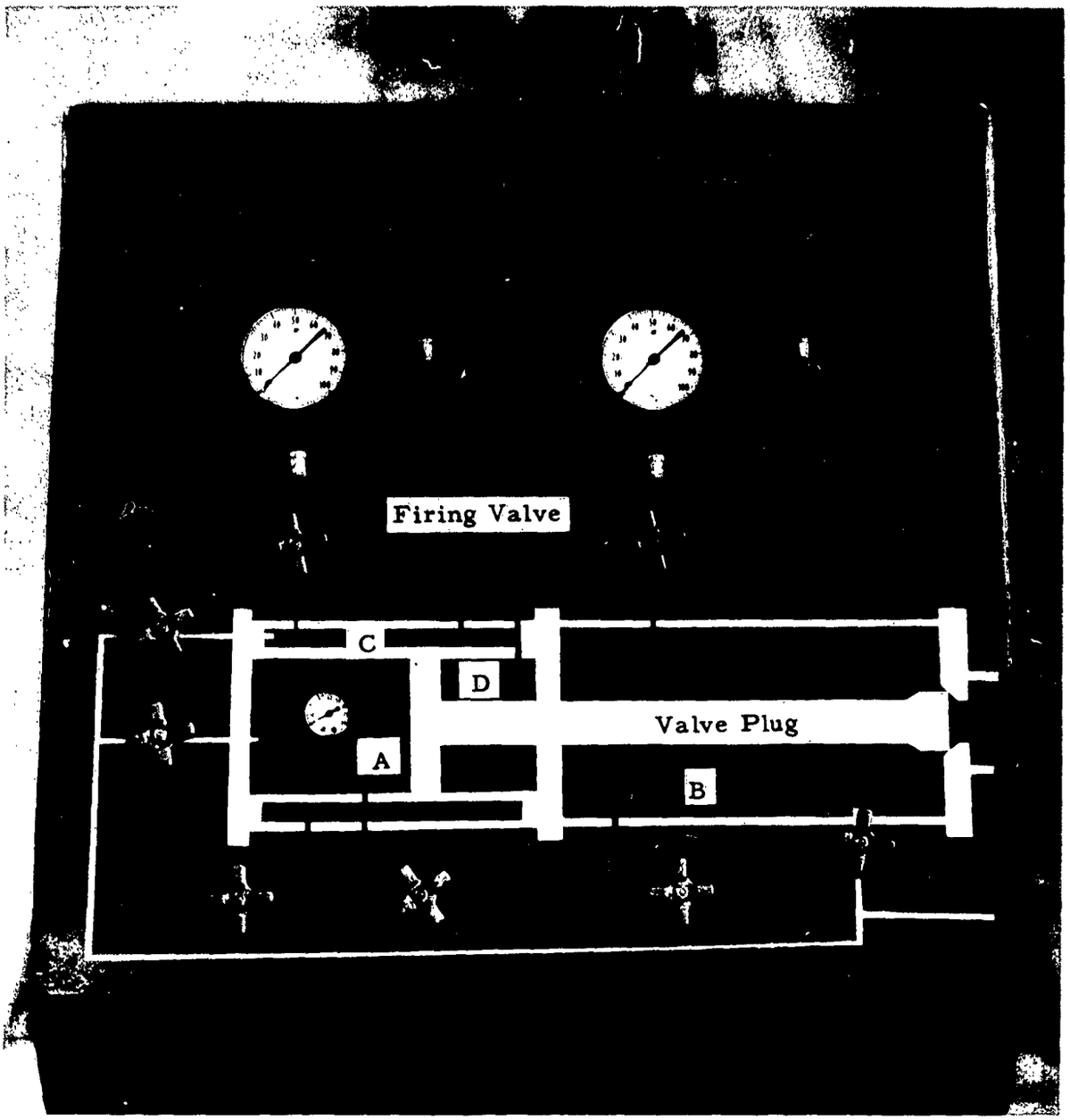

Fig. 3. Control Panel for 4-In.-Bore Air Gun.

Cylinders weighing 54 and 78 lb were used as acceleration masses during the course of the study. A 6-in. -long concrete specimen weighed approximately 5 pounds. Thus the total mass accelerated by the impact of the projectile was either 79 or 103 pounds. After impact, the entire assembly was caught in a cushion of paper honeycomb. Details of the assembly are clearly shown in Figs. 2 and 4. Note that the projectile is fired directly into the specimen and is 4 in. in diameter as compared to the 6-in. - diameter cushion.

Measurements

Velocity. Velocity measurements were made by recording the output of a magnetic pickup device installed 1 in. from the end of the gun barrel. Two sharp voltage peaks, produced by machined grooves in the projectile as it moved past the magnetic pickup, were recorded as a function of time on a Polaroid camera-equipped Tektronix Type 535 oscilloscope.

Acceleration. The impact acceleration of the mass-cushion system was measured with a Statham Model A5-500-350 accelerometer having an operating range of $\pm$ 500g, a natural frequency of approximately 2000 cps, and a damping factor of approximately 0. 60 of critical value. The accelerometer was bolted rigidly to the rear of the acceleration mass as shown in Figs. 2 and 4. The accelerometer was protected with two wooden blocks bolted to the mass. A Tektronix Type 535 oscilloscope, equipped with a Polaroid Camera, was used to record the acceleration as a function of time. Some typical records are shown in Fig. 5.

The sensing element in a Statham accelerometer consists of an unbonded, four-element, strain-sensitive, resistance-wire network which may be

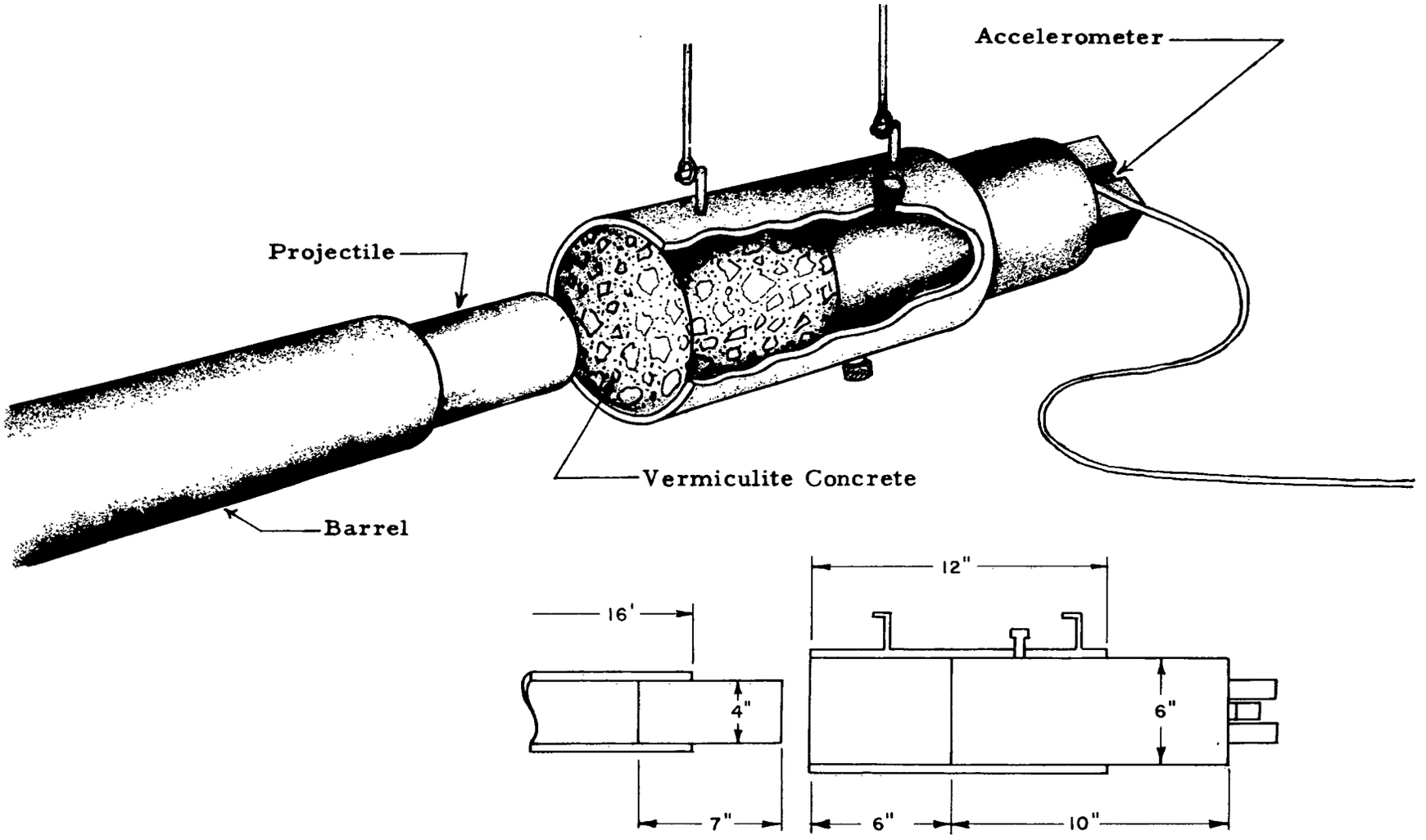

Fig. 4. Acceleration Apparatus Showing Confined Vermiculite Concrete and Various Components

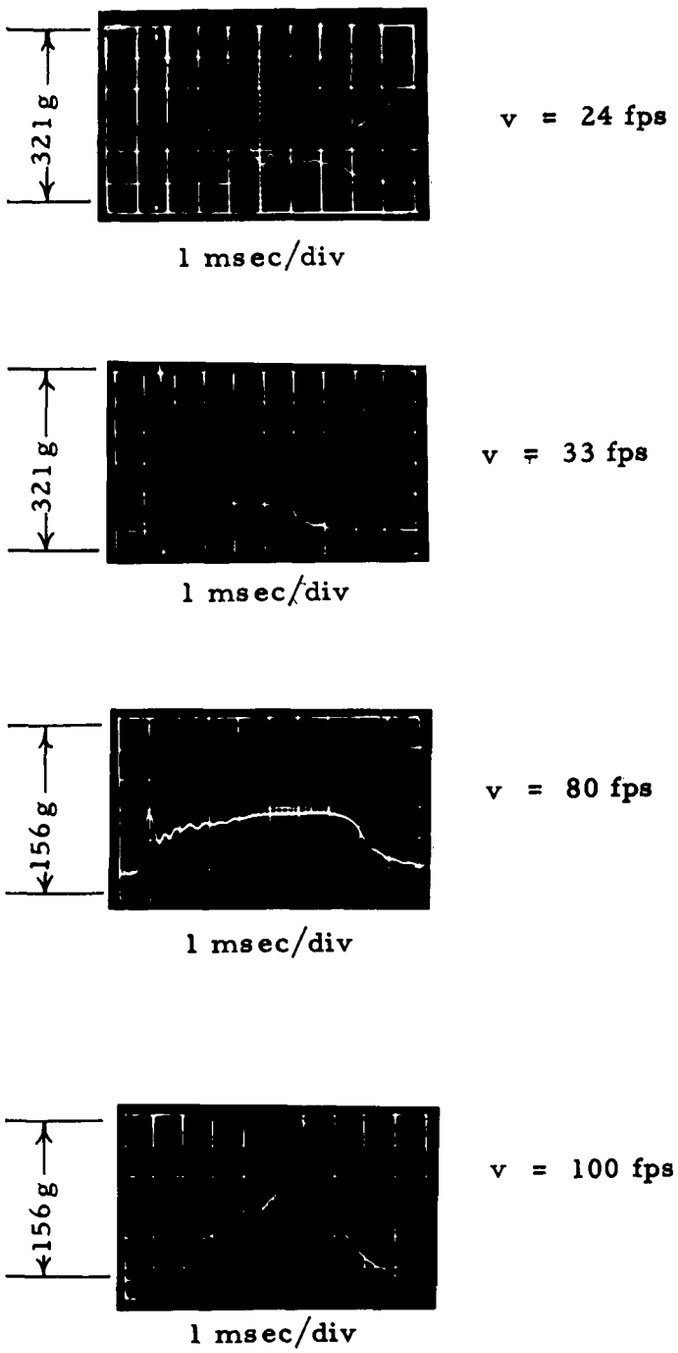

Fig. 5. Typical Acceleration-Time Records.

represented electrically by a Wheatstone bridge.

The accelerometer is calibrated by connecting a resistor across one arm of the transducer bridge. A deflection in the output circuit results which corresponds to the effect of the combined resistance changes in the bridge arms due to a change in acceleration.

Reliability of Measurements

Several checks were made to insure the reliability of the acceleration-time measurements.

First, a check was made on the data by using conservation of Momentum principles. The final velocity of the cushioned system may be calculated from the equation

$$V_f = \frac{M_p V_o}{M_p + M_m} \qquad \text{- - - - - (1)}$$

where V_f = Final velocity of projectile-cushion system

V_o = Impact velocity of projectile

M_m = The cushioned mass

M_p = The projectile mass

Since the area under the acceleration-time curve represents the change in velocity of the cushioned system, V_f may also be found from

$$V_f = \int a_m dt \qquad \text{- - - - - (2)}$$

A comparison of (1) and (2) was made for each impact velocity, and the results are shown in Table I.

A second check was made by comparing the maximum strain indicated on the stress-strain curves to permanent strain measured after each impact. This comparison checked reasonably close.

TABLE I

COMPARISON OF THEORETICAL AND MEASURED RESULTS

Impact Velocity fps	$V_f = \int a_m dt$	$V_f = \frac{M_m V_o}{M_p + M_m}$
24	4.9 4.6	4.7 4.7
33	6.6 6.6	6.5 6.5
40	8.0 7.6	7.8 7.8
49	9.9 9.5	9.6 9.6
60	10.8 11.1	11.7 11.7
80	15.3 14.7	15.6 15.6
100	20.3 20.1	19.5 19.5
120	23.5 22.3	23.4 23.4

A further check of the data was made by substituting a 74-lb acceleration mass for the 98-lb mass, used in the bulk of the investigation and making a series of shots at 60 fps. This made the total weight of the accelerated system 79 lb instead of 103 pounds. From Newton's Second Law, the accelerations measured should be inversely proportional to the ratio of the acceleration mass weights. Fig. 6 shows two typical acceleration-time records taken from this series of impacts.

A theoretical response curve for an input acceleration of 50g was calculated for the accelerometer to determine what portion of the initial peak could be attributed to the accelerometer itself. The theoretical-response curve and method of calculation are included in Appendix B.

The results of these four checks on the data validify the results and indicate that full confidence can be placed in the material properties measured.

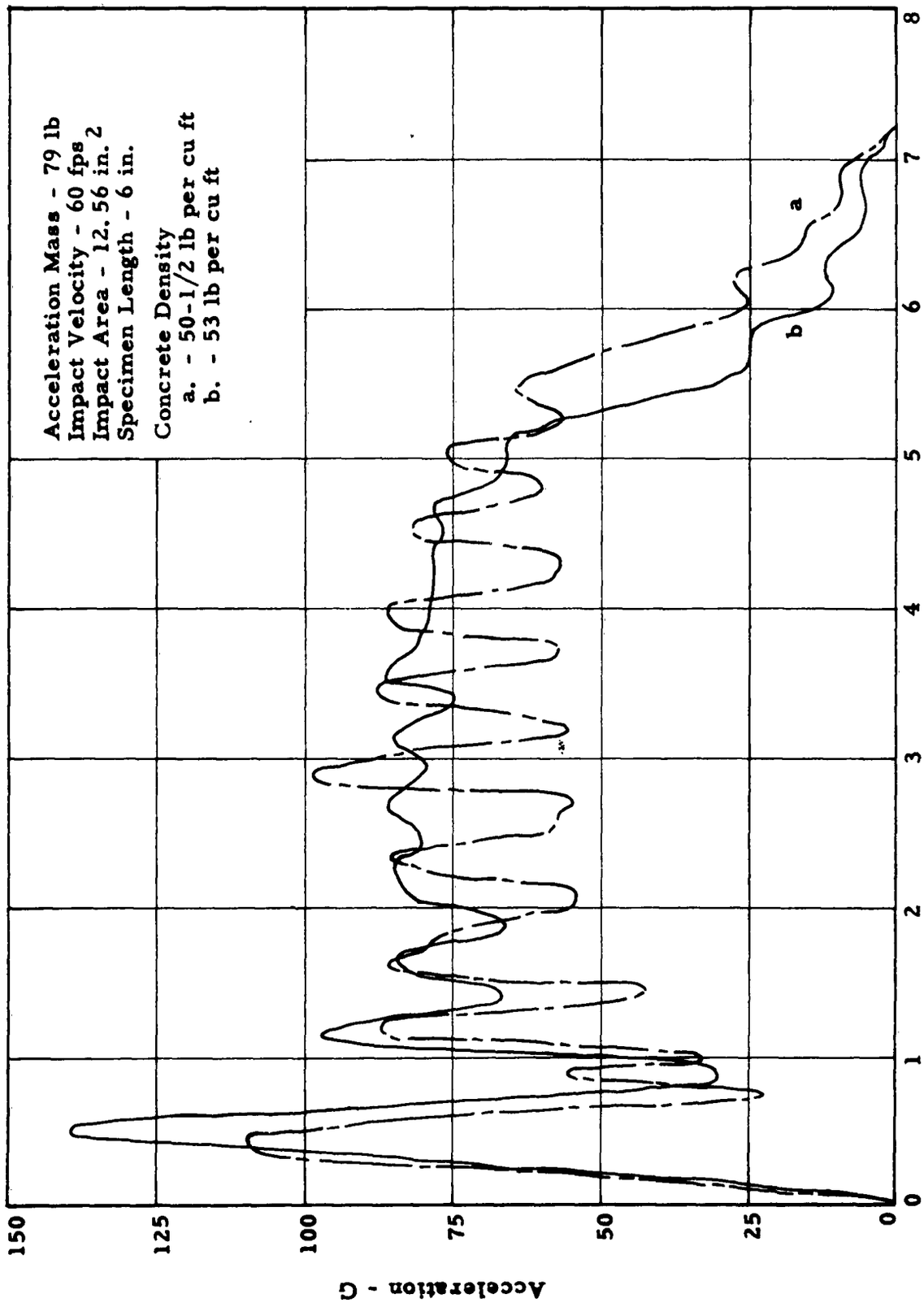

Fig. 6. Acceleration-Time Curves for 79-lb Acceleration Mass

DISCUSSION OF RESULTS

General Characteristics of the Curves

The acceleration-time curves recorded photographically from an oscilloscope at impact, and the corresponding stress-strain curves obtained by integration are shown in Figs. 7 through 22 for a total of 16 impacts made using a 4-in.-bore air gun. Each figure has two curves made under identical conditions to show the extent that data are reproducible.

The acceleration-time curves, and consequently the stress-strain curves, have initial peaks, the magnitudes of which are considerably greater than the average. As previously mentioned in the Introduction, the question of whether this peak is caused by the data-measuring instrumentation or technique, or is attributable to some other cause is of some concern. When the damping characteristics of the accelerometer used in this study are considered (See Appendix B), it appears probable that a part of the initial acceleration peak is caused by the accelerometer. The theoretical-response curves developed on a computer for the accelerometer indicate an "overshoot" on the initial part of a square wave of as much as 6 per cent. The theoretical overshoot is not nearly as great as the initial peak consistently recorded experimentally, however. It appears likely that some of the initial peak recorded is the result of action in the lightweight concrete itself.

It may be seen in Figs. 19 and 21 that the cushioning material "bottoms" when an insufficient amount is used, and that consequently the acceleration increases rapidly near the end of the impact.

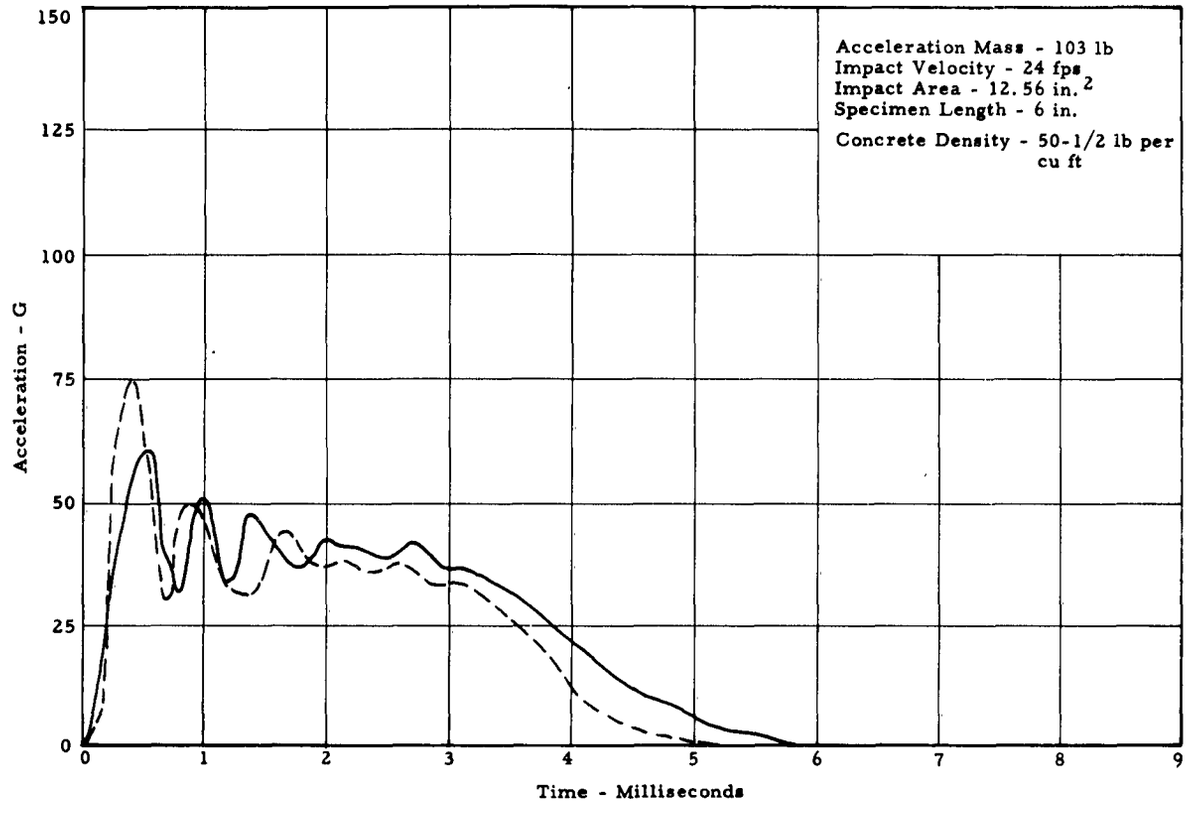

Fig. 7. Acceleration-Time Curves for 24 fps Impact Velocity

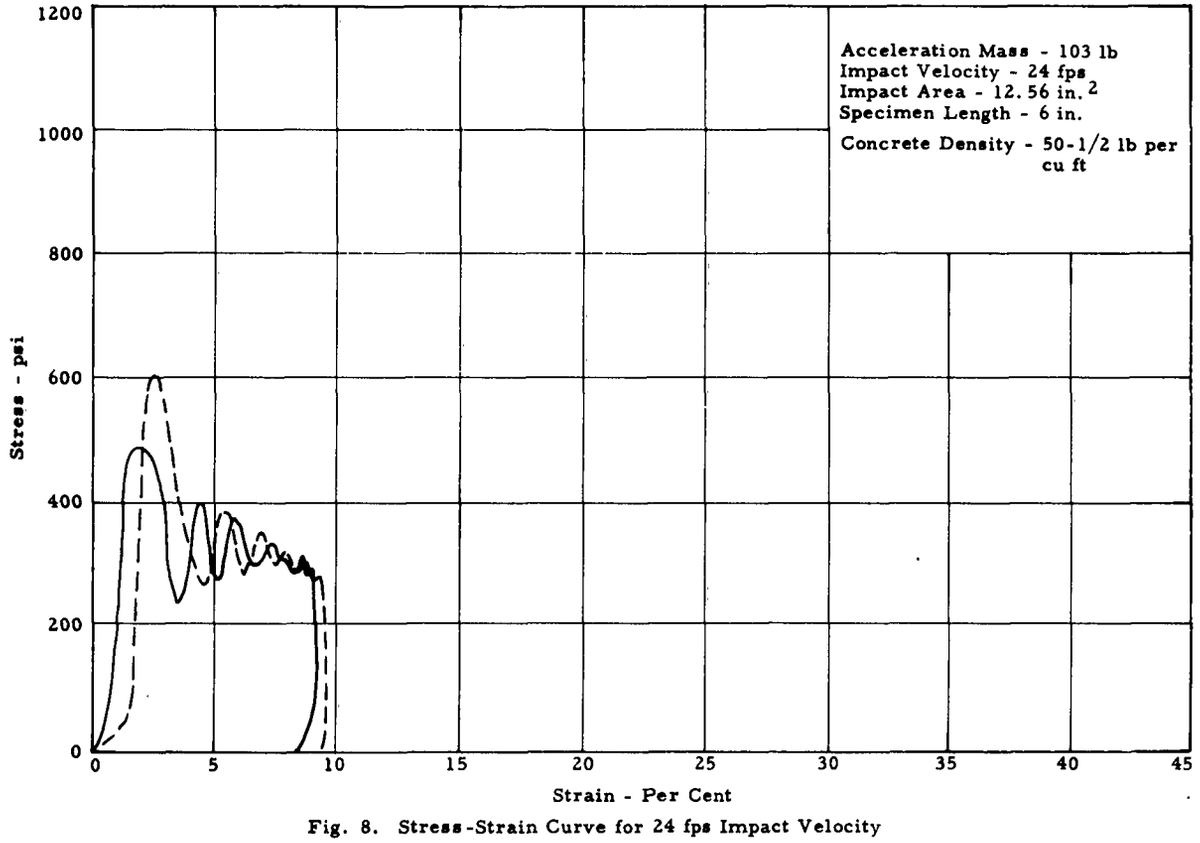

Fig. 8. Stress-Strain Curve for 24 fps Impact Velocity

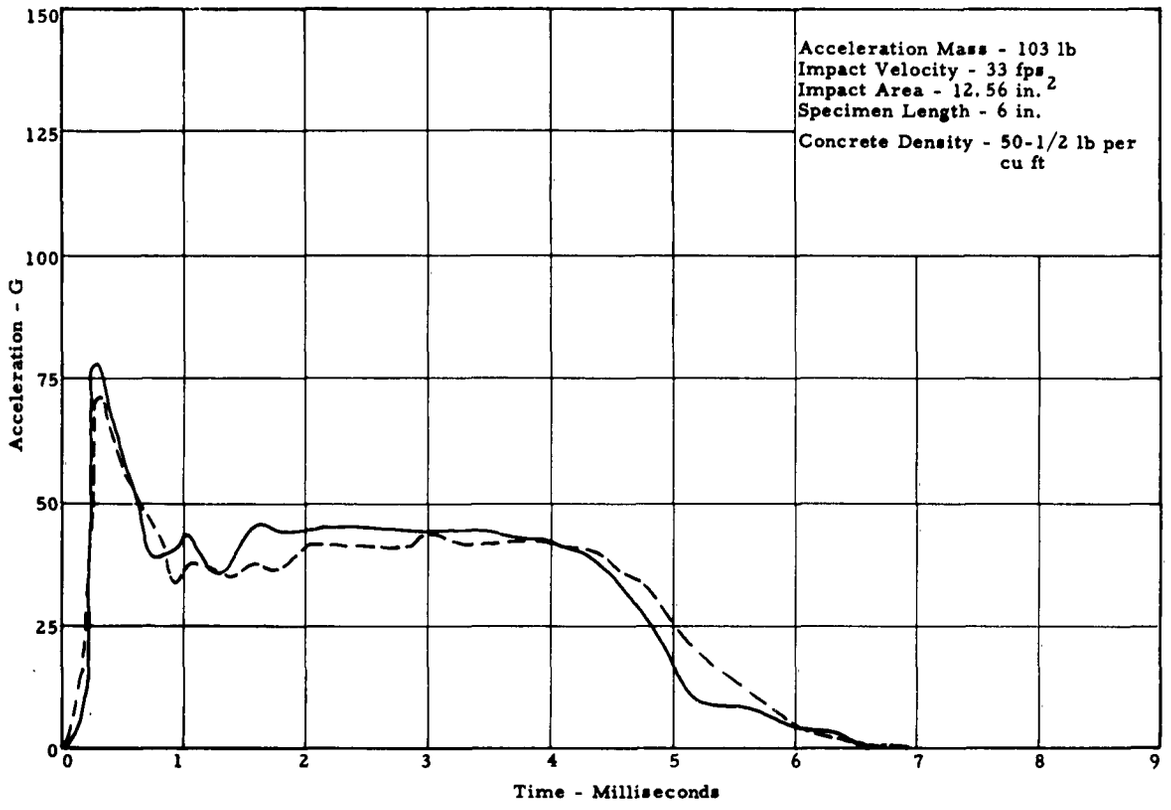

Fig. 9. Acceleration - Time Curves for 33 fps Impact Velocity

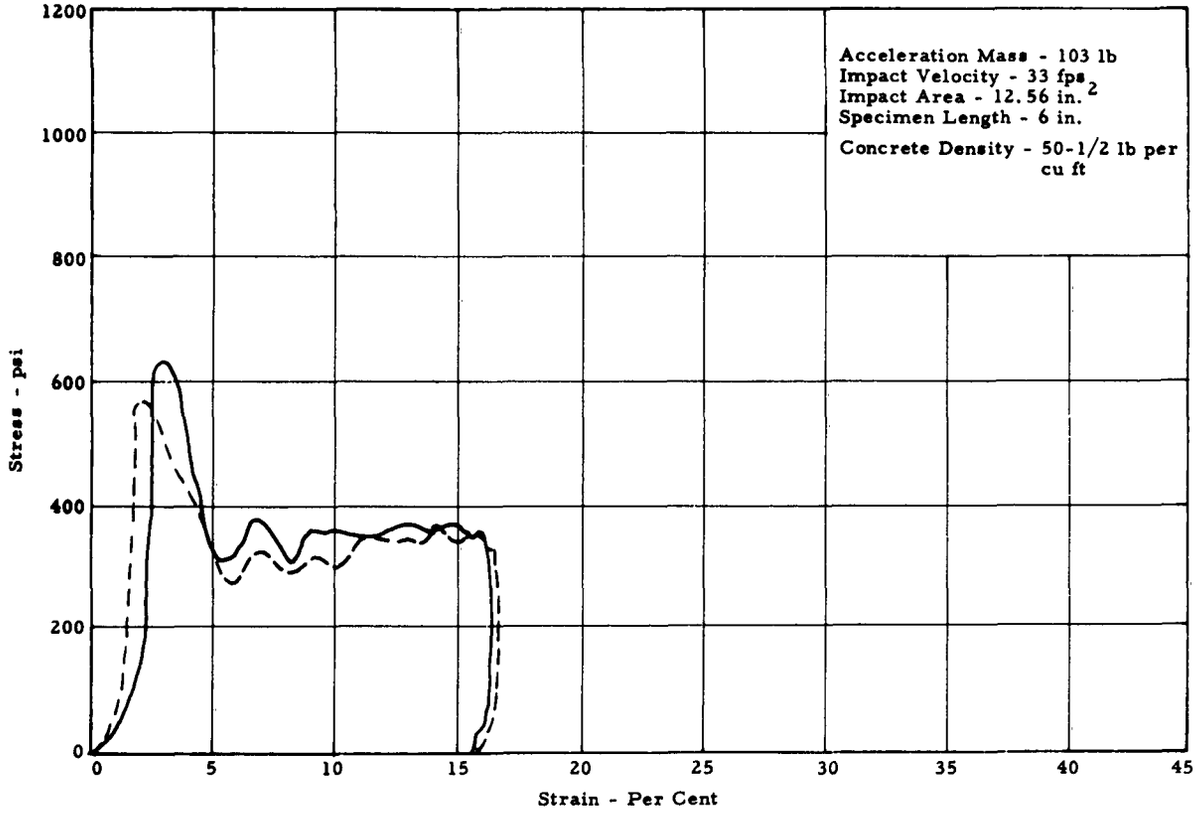

Fig. 10. Stress-Strain Curve for 33 fps Impact Velocity

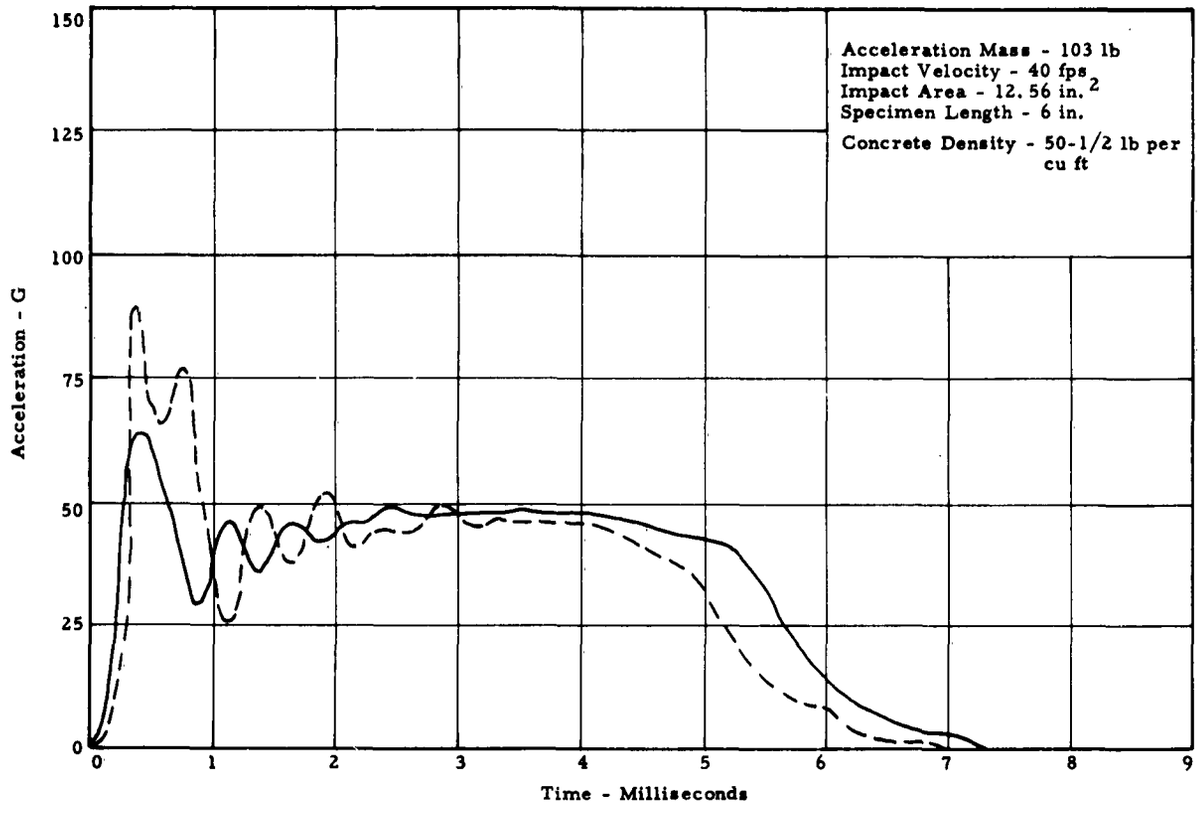

Fig. 11. Acceleration - Time Curves for 40 fps Impact Velocity

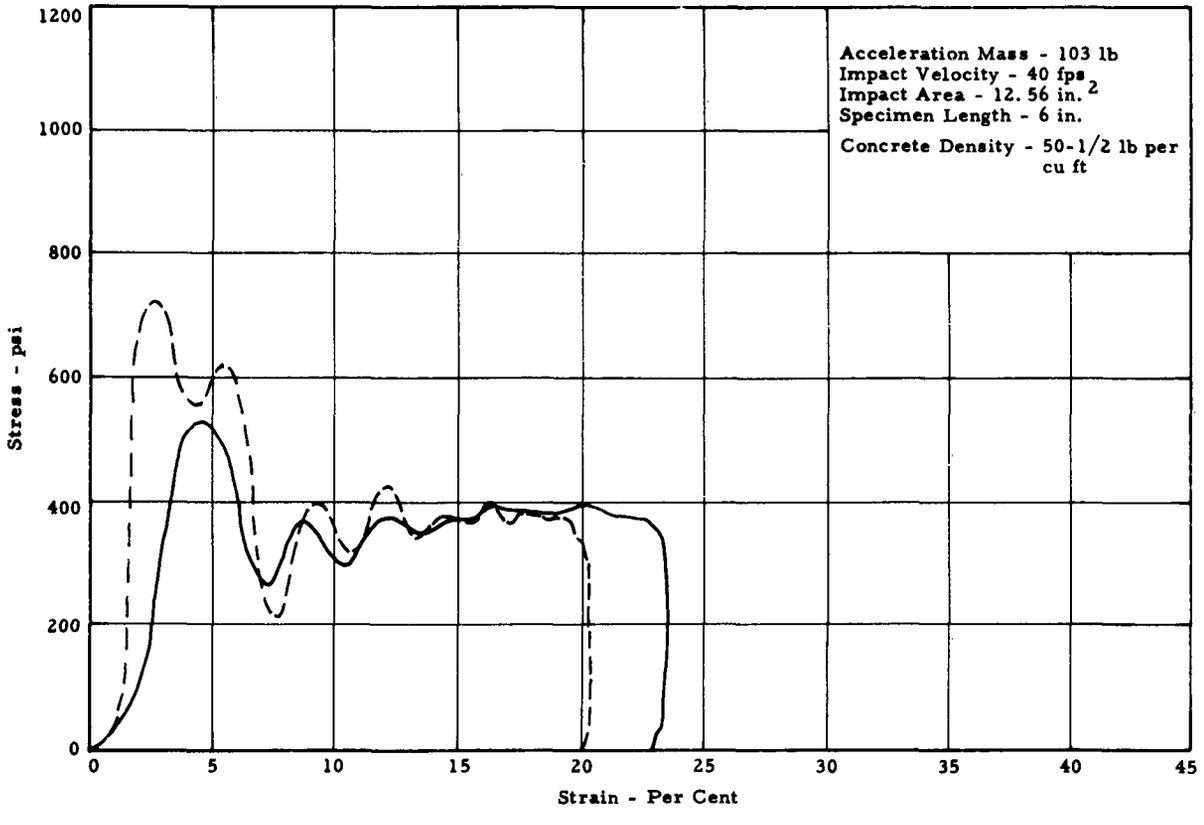

Fig. 12. Stress-Strain Curve for 40 fps Impact Velocity

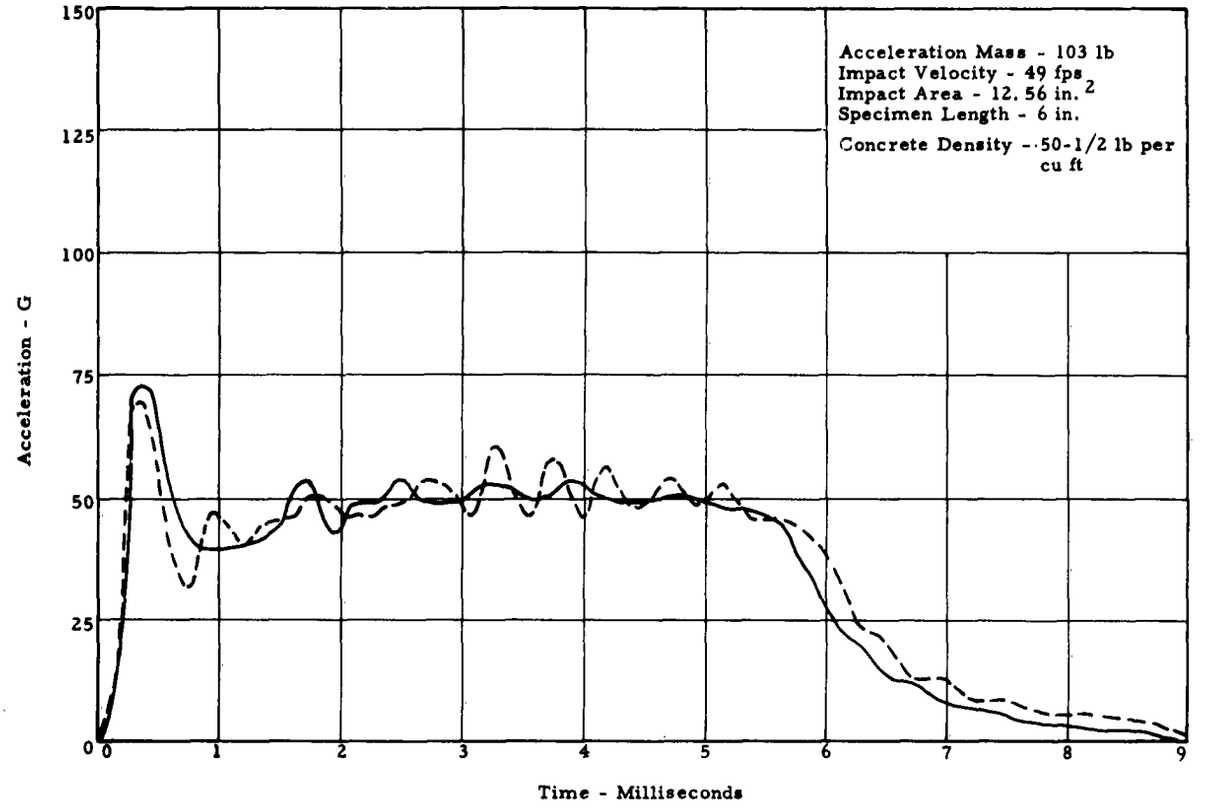

Fig. 13. Acceleration-Time Curves for 49 fps Impact Velocity

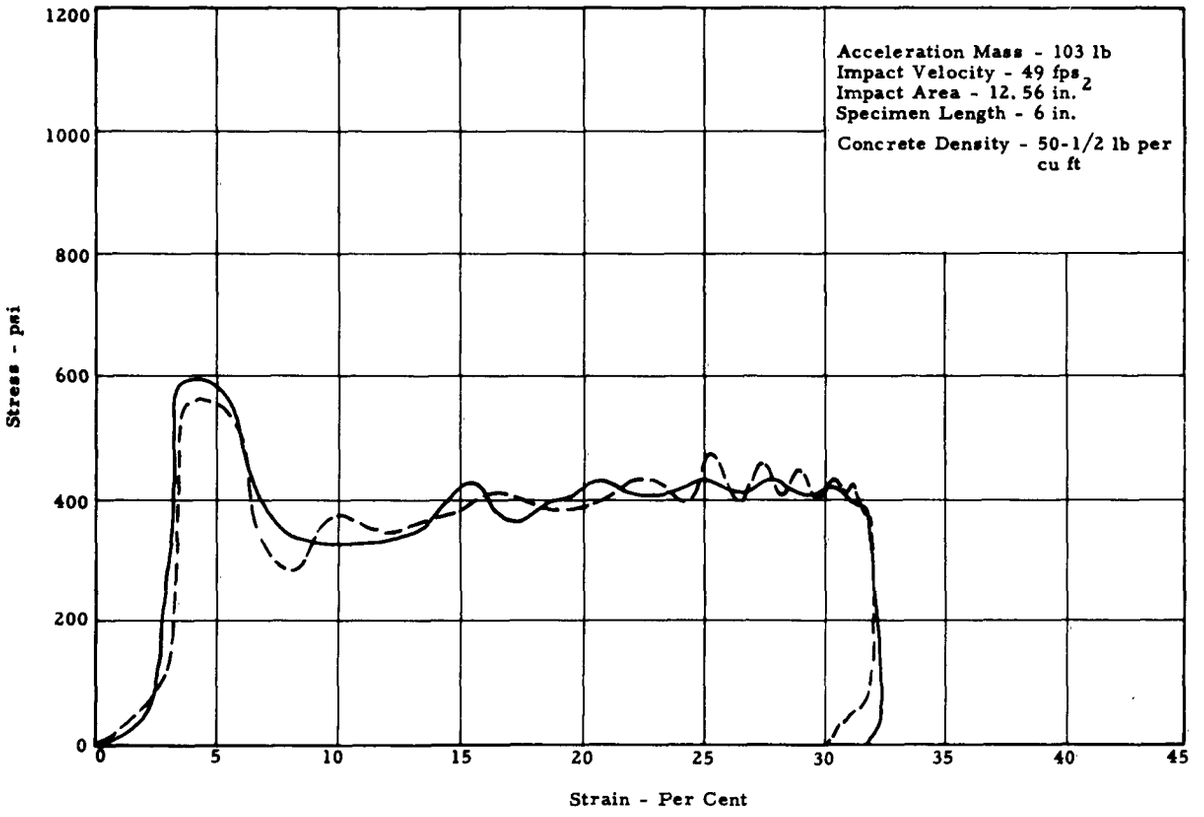

Fig. 14. Stress-Strain Curve for 49 fps Impact Velocity

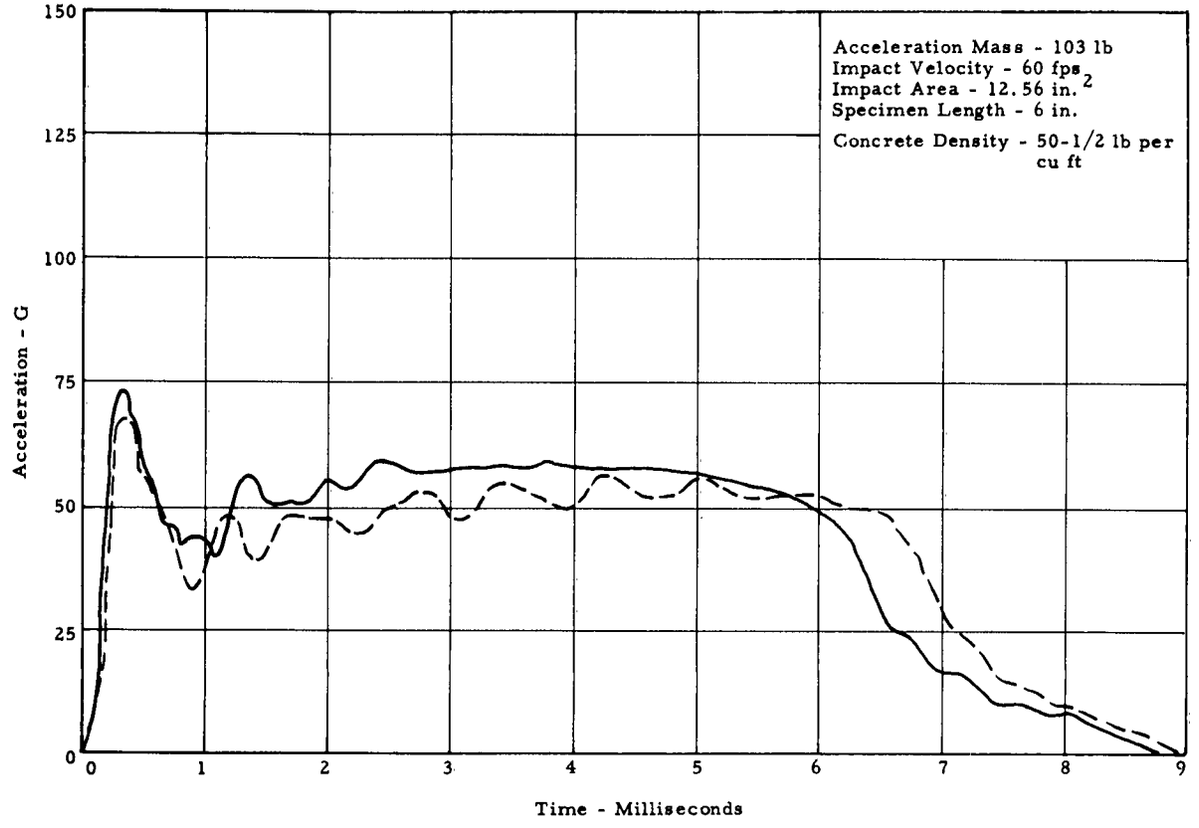

Fig. 15. Acceleration-Time Curves for 60 fps Impact Velocity

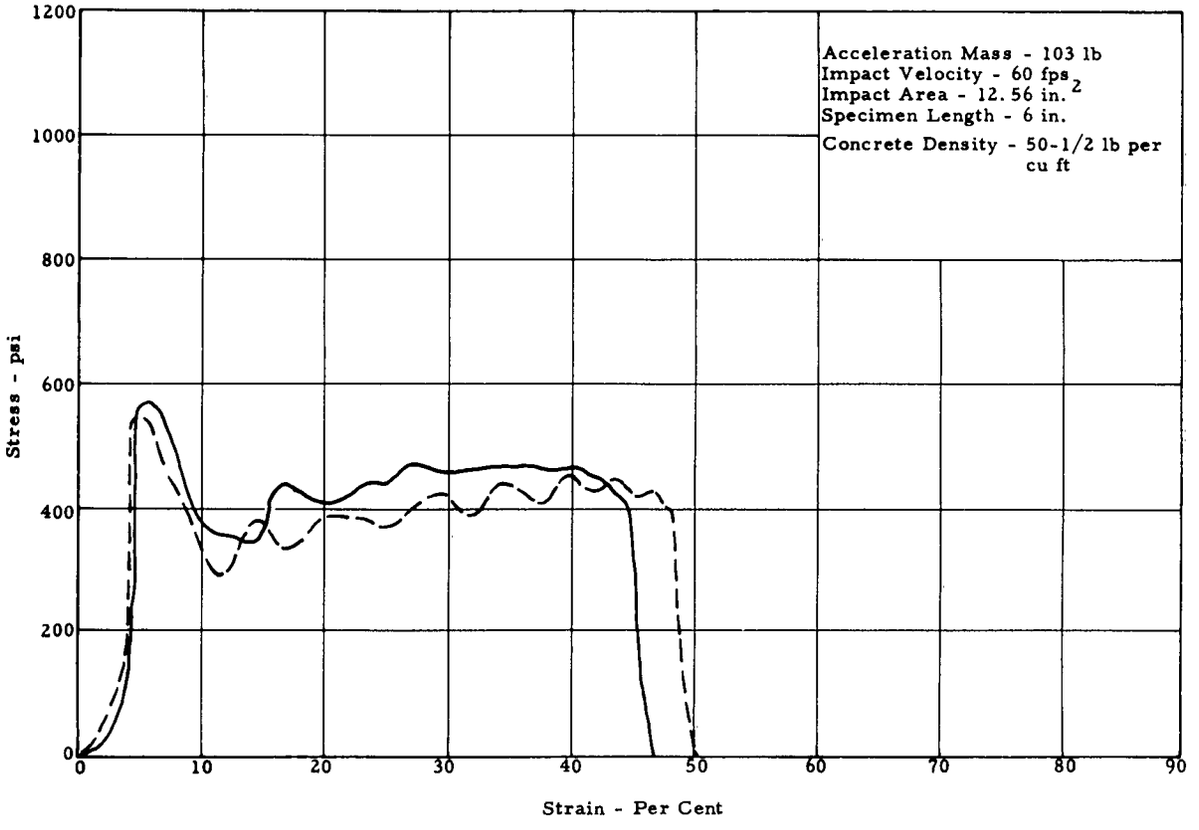

Fig. 16. Stress-Strain Curve for 60 fps Impact Velocity

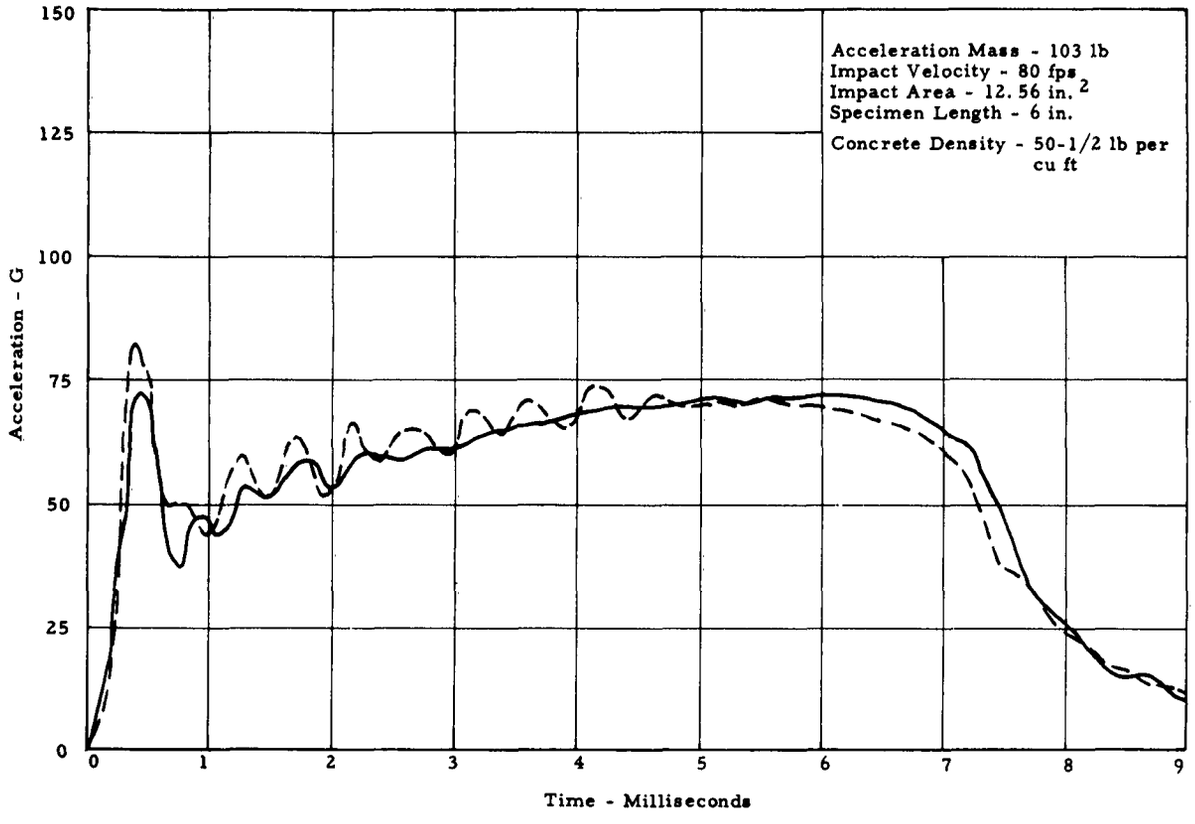

Fig. 17. Acceleration-Time Curves for 80 fps Impact Velocity

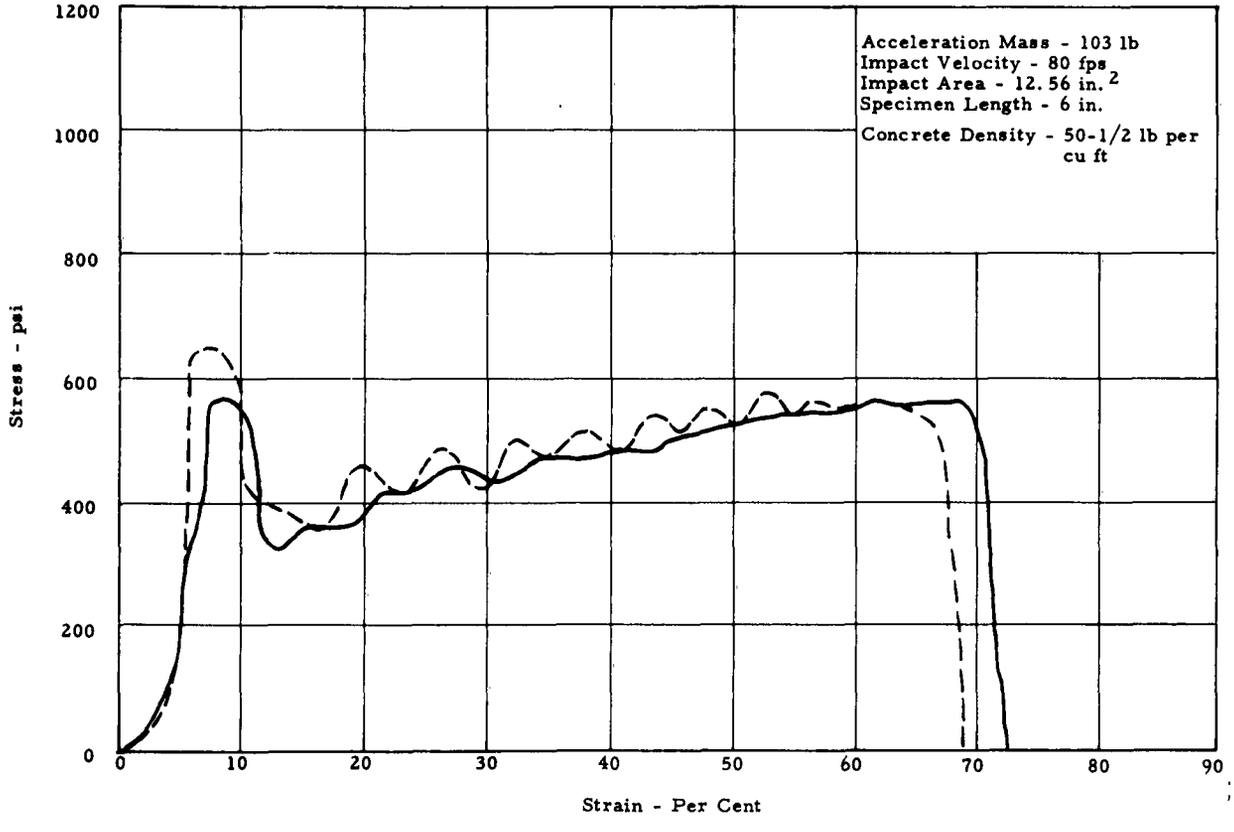

Fig. 18. Stress-Strain Curve for 80 fps Impact Velocity

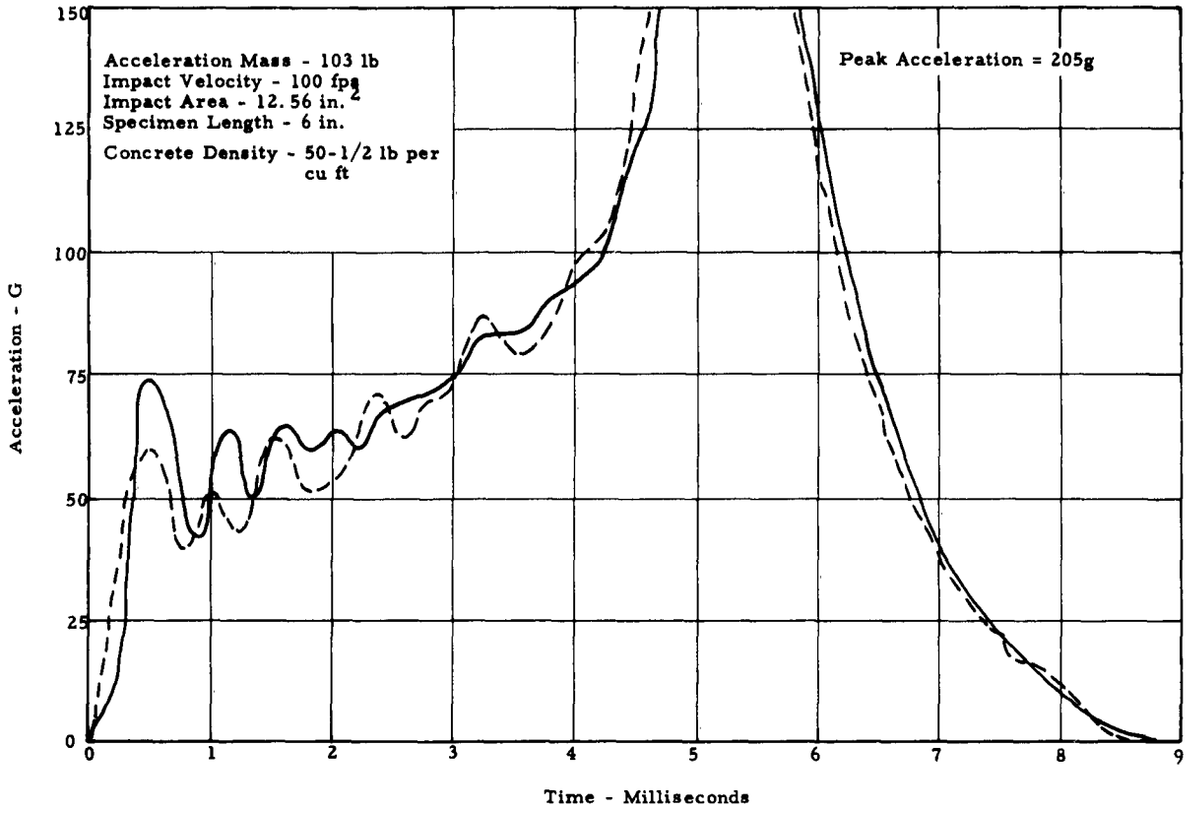

Fig. 19. Acceleration-Time Curves for 100 fps Impact Velocity

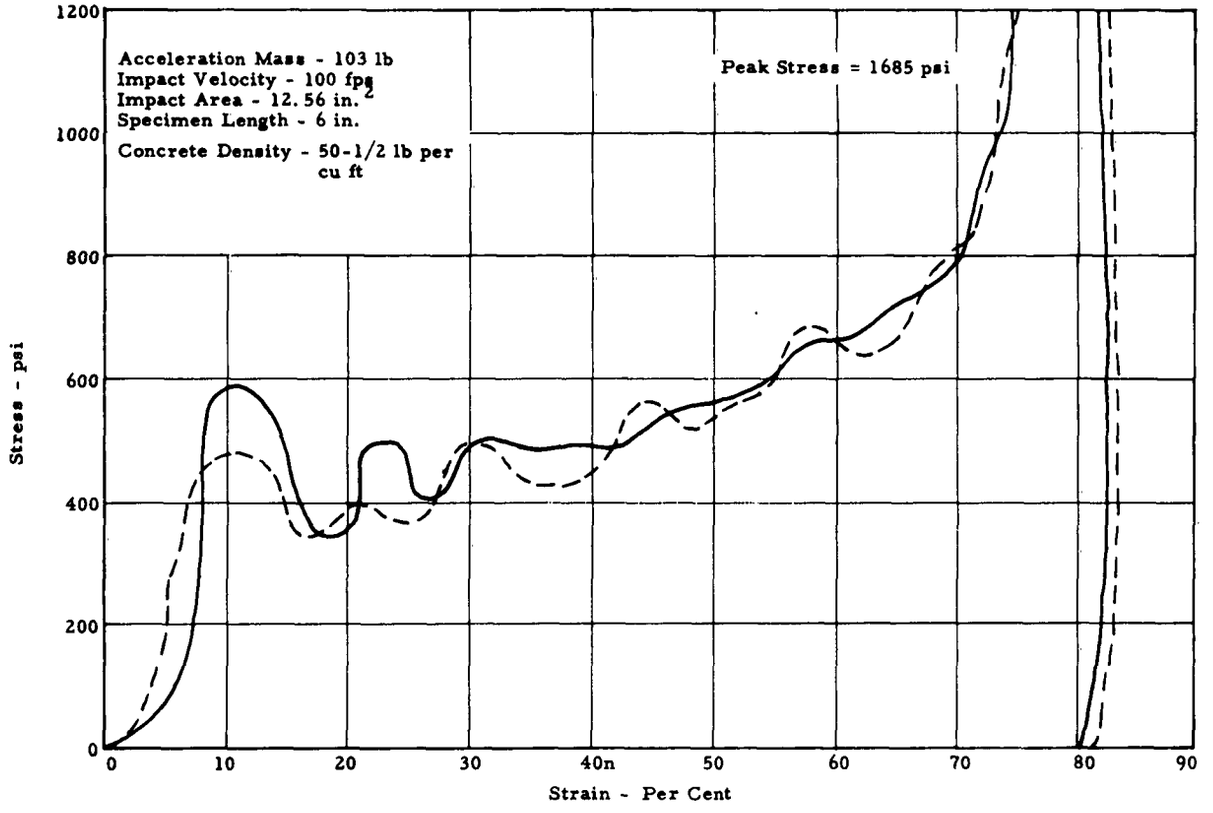

Fig. 20. Stress-Strain Curve for 100 fps Impact Velocity

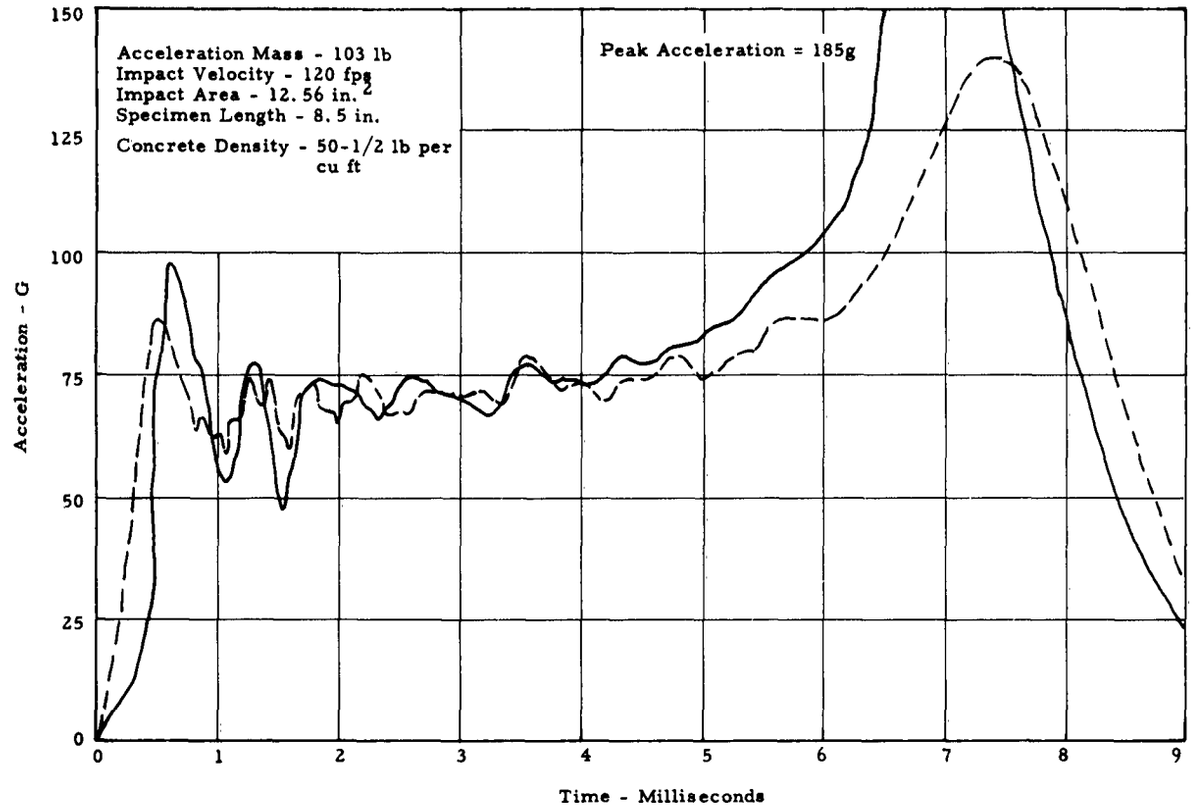

Fig. 21. Acceleration - Time Curves for 120 fps Impact Velocity

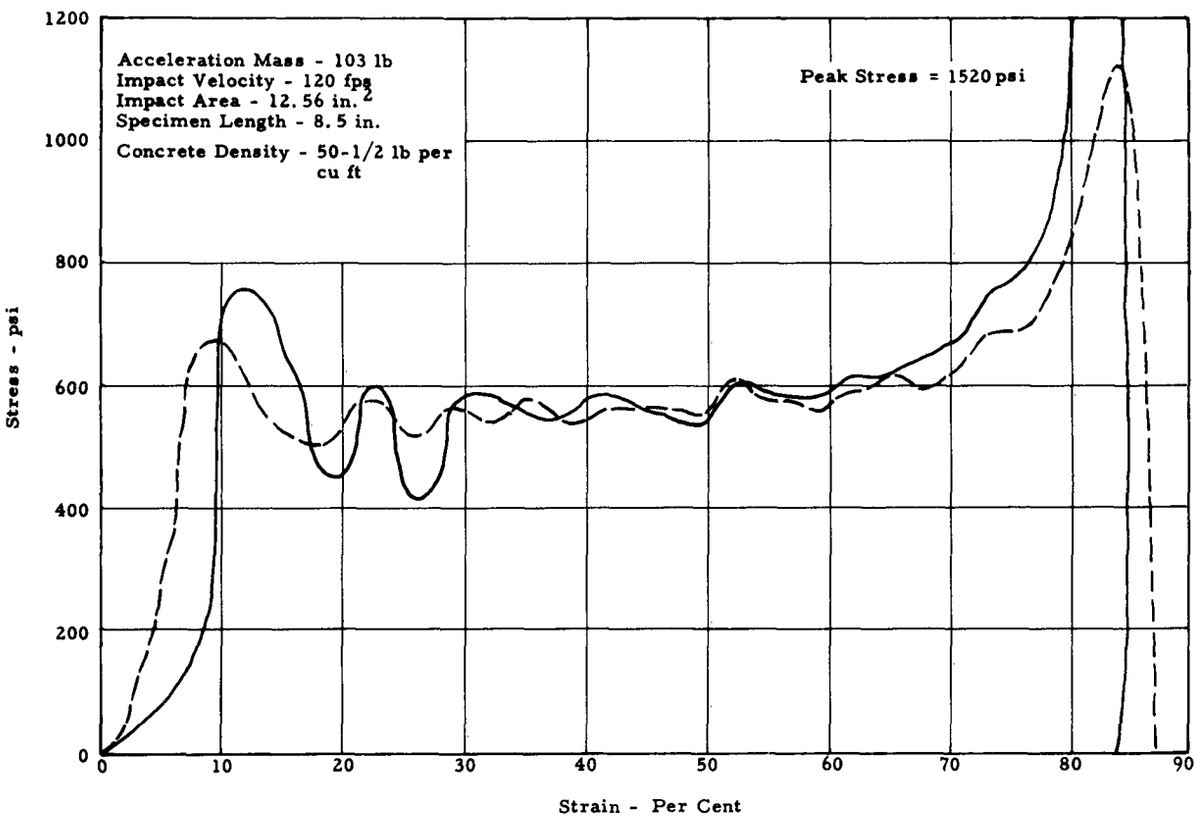

Fig. 22. Stress-Strain Curve for 120 fps Impact Velocity

Effect of Impact Velocity

Both the initial peak crushing stresses and the average crushing stresses were obtained from the stress-strain curves for the various tests and plotted against impact velocity as shown in Fig. 23. The average crushing stresses were selected from the stress-strain curves out to the point where bottoming began. A straight-line fit was applied to the plotted points in Fig. 23 to obtain the solid lines. Data obtained by Covington[2] are shown, for comparison, by broken lines in Fig. 23. The stress shown at zero velocity is the stress corresponding to the average static crushing stress. Summary plots of some of the acceleration-time curves and the corresponding stress-strain curves are shown in Figs. 24 and 25, respectively, to aid in comparing the results.

The stress-strain and stress-time curves obtained at the drop tower consistently show a second peak which is higher in magnitude than the initial peak. Typical stress-strain and stress-time curves from the drop tower data are shown, for comparison, in Figs.26 and 27. A static stress-strain curve for the confined concrete is also shown, for comparison, in Fig. 26. The confining technique used to obtain the static data is described in detail by Covington.[2] It has been shown by Tapley[3] that the natural vibration of the dynamometer-force-plate system causes oscillations which distort the impact records. It is possible that these two peaks are actually a single-stress peak separated by oscillations in the dynamometer. The theoretical response curves (See Appendix B) for the accelerometer show that a portion of the initial peak in a record obtained with the air gun is due to the "overshoot" of the accelerometer. These two phenomena may account

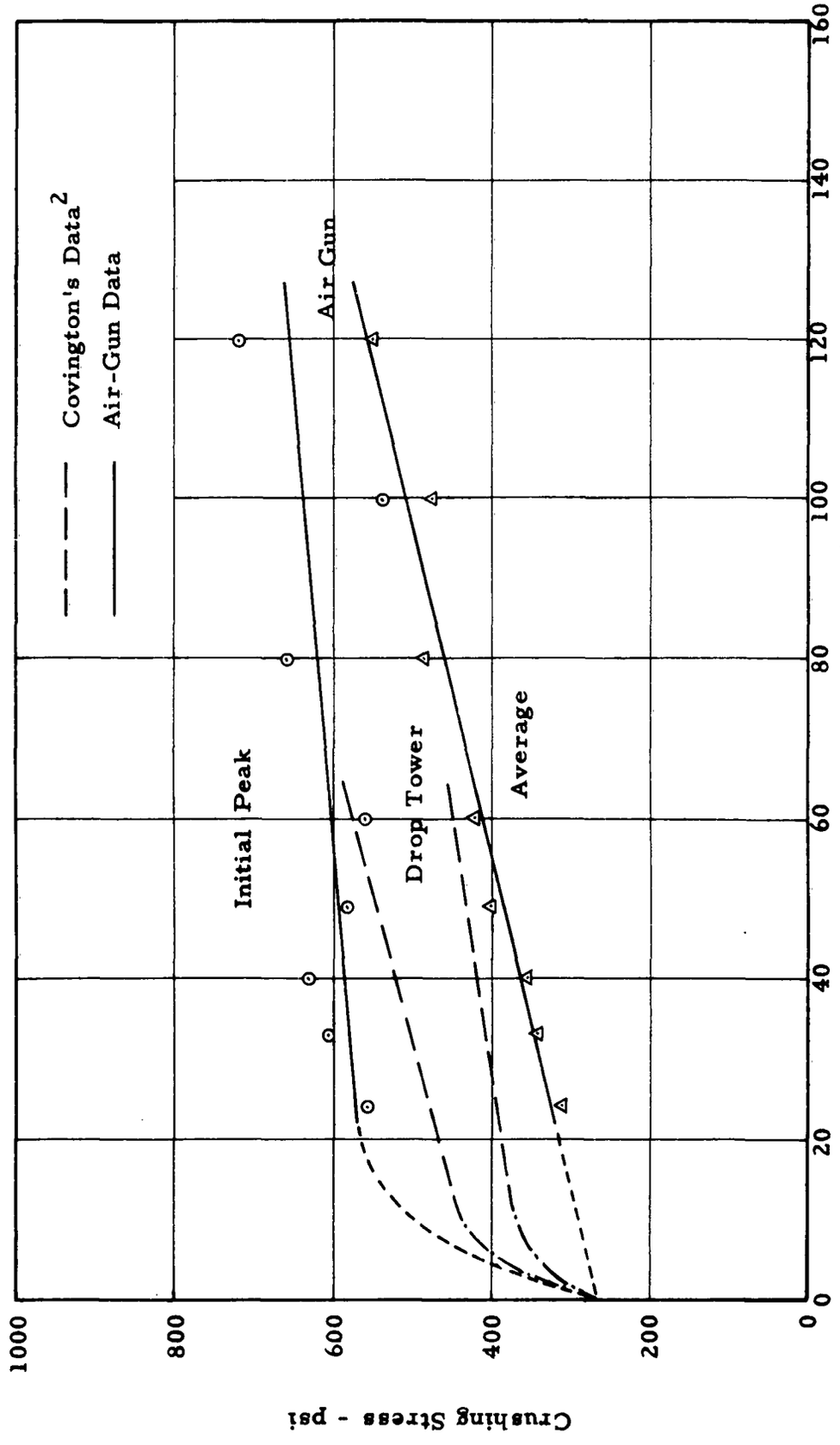

Fig. 23. Effect of Impact Velocity on Crushing Stress.

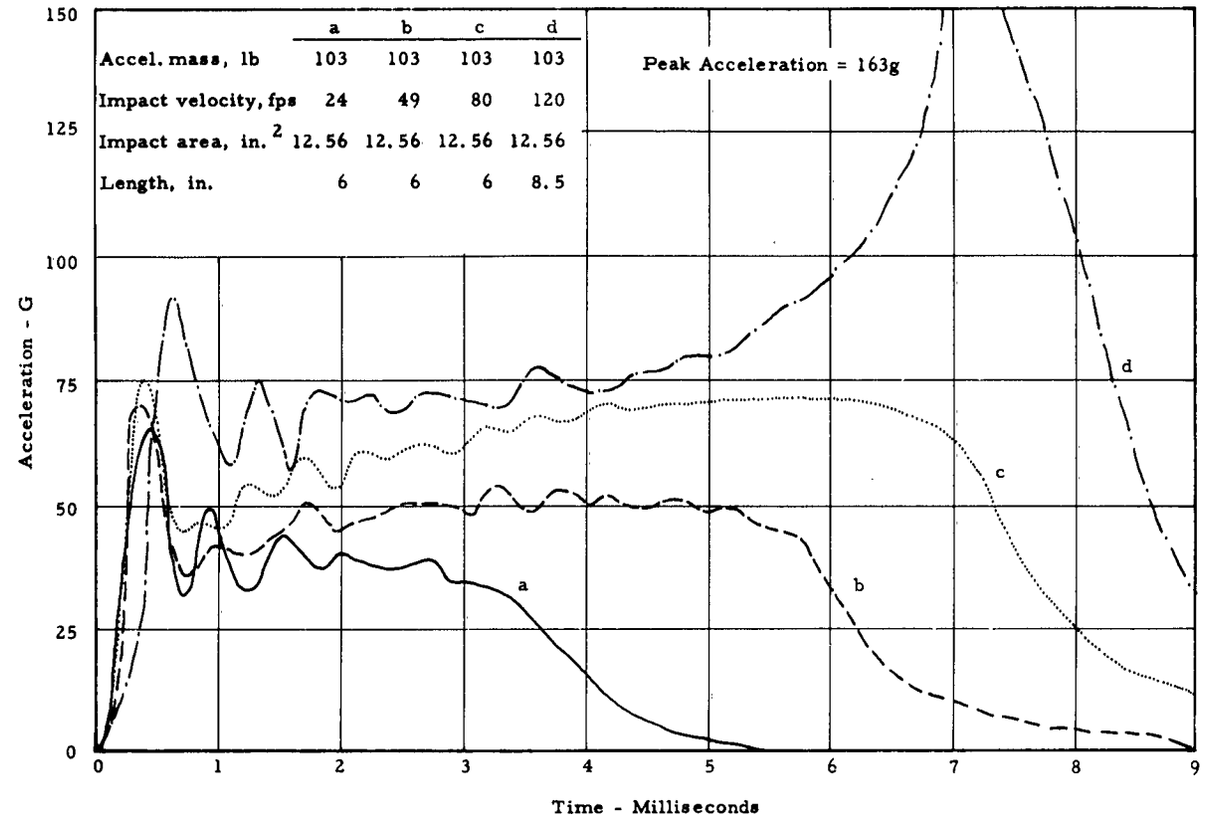

Fig. 24. Acceleration-Time Curves Showing Effect of Impact Velocity

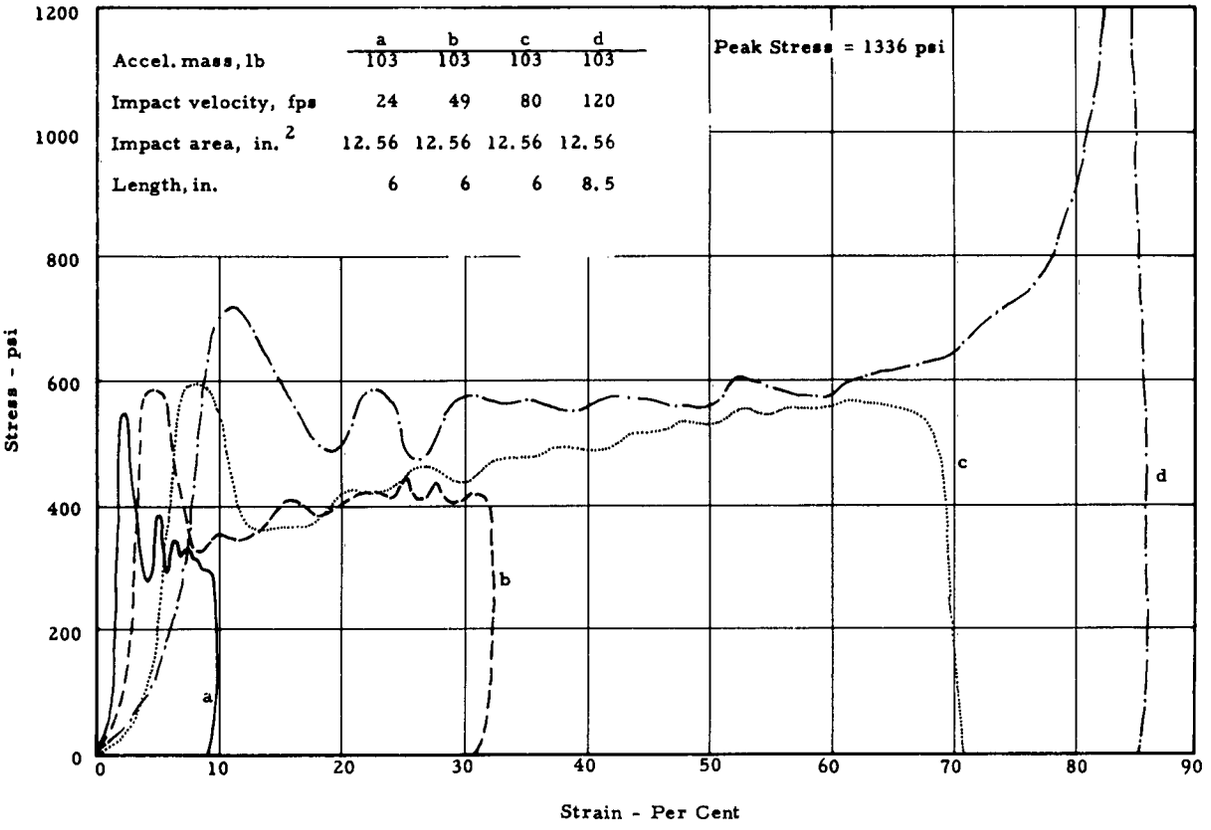

Fig. 25. Stress-Strain Curves Showing Effect of Impact Velocity.

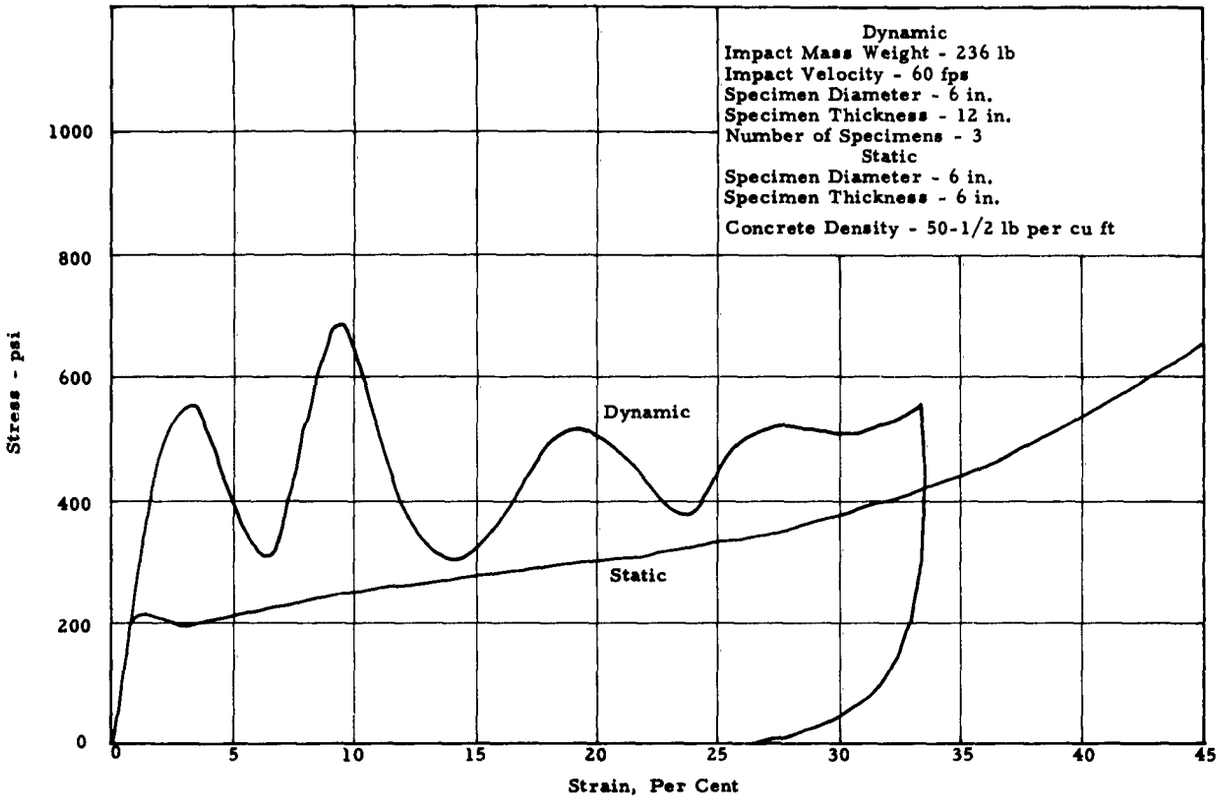

Fig. 26. Static Stress-Strain Curve and Typical Stress-Strain Curve from Tower Data

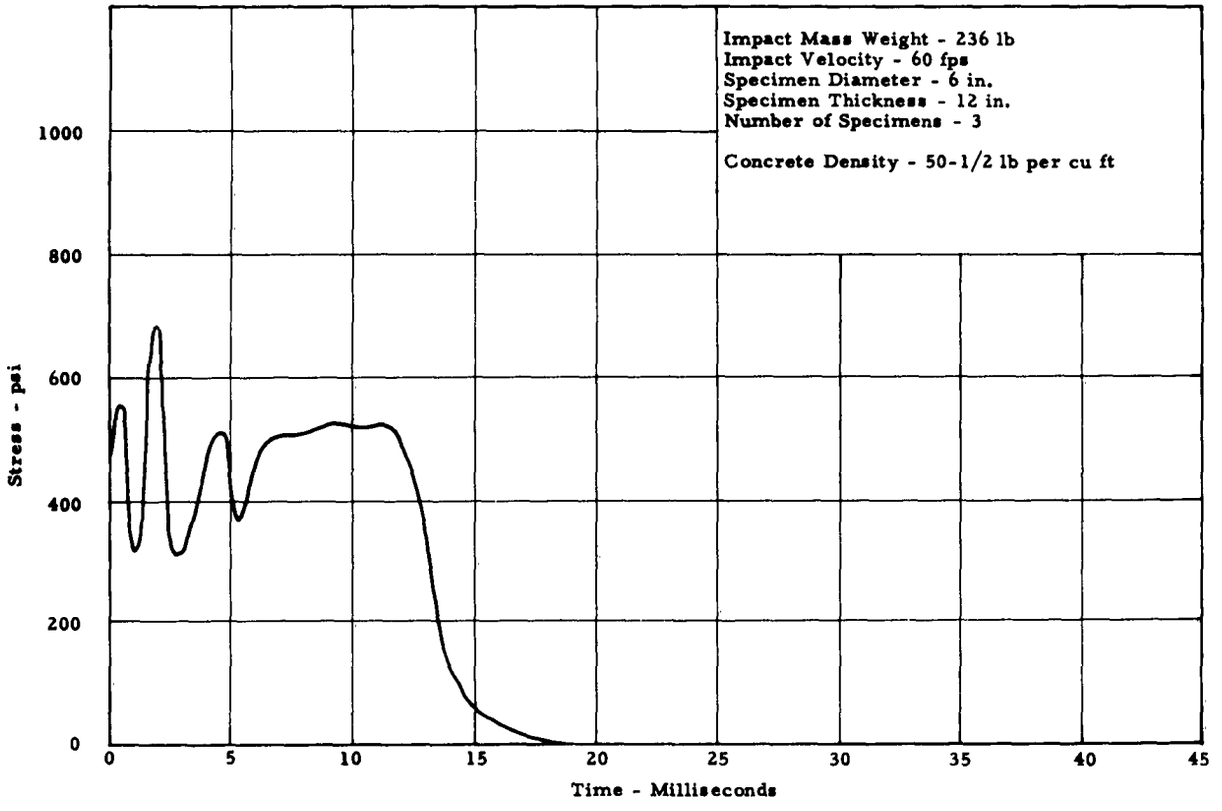

Fig. 27. Typical Stress-Time Curve from Tower Data

for the difference in the data obtained by the different techniques.

In any case, it appears, from the results obtained in this study, that the usual method[3] of "averaging" out the oscillations in the dynamic stress-strain curves should not be used when data other than energy absorption is of primary interest.

From the trend of the data shown in Fig. 23, it appears that the initial peak crushing stress will not continue to increase at the same rate with impact velocity, but will approach the average crushing stress at higher velocities. A study of the effect of higher impact velocities would, of course, provide more conclusive results. Considering the two different data-measurement techniques and the two different data-reduction methods necessary to obtain the stress-strain curves from acceleration-time curves, the correlation between the two studies is quite close.

A comparison of the stress-strain curves obtained from the drop-tower data and the air-gun data, both at the same concrete density and impact velocity is shown in Fig. 28. It can be seen that the average stress of each curve is about the same up to about 35 per cent strain.

Effect of Cushioning Thickness

Figures 29 and 30 show the effects on the acceleration-time curve of progressively decreasing the available cushioning thickness while maintaining a constant energy-input level. An interesting comparison may be made with Figs. 19 and 21 in which the input energy was increased while the cushioning thickness remained constant. In each case, the cushioning-material volume reached a point where it was insufficient to cushion the acceleration mass without, "bottoming" occurring. It is very significant

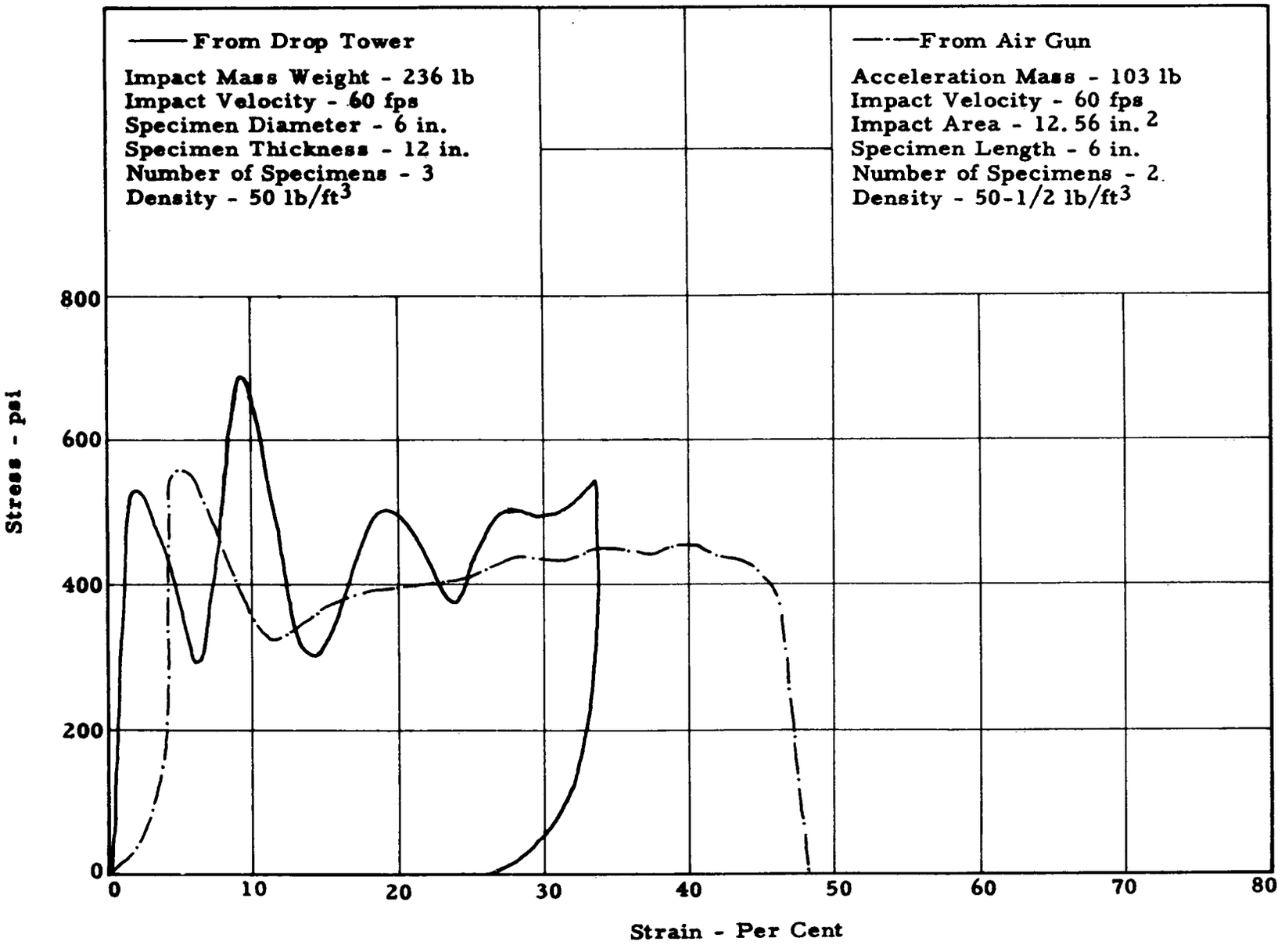

Fig. 28. Stress-Strain Curves for Same Impact Velocities from Drop Tower and Air Gun.

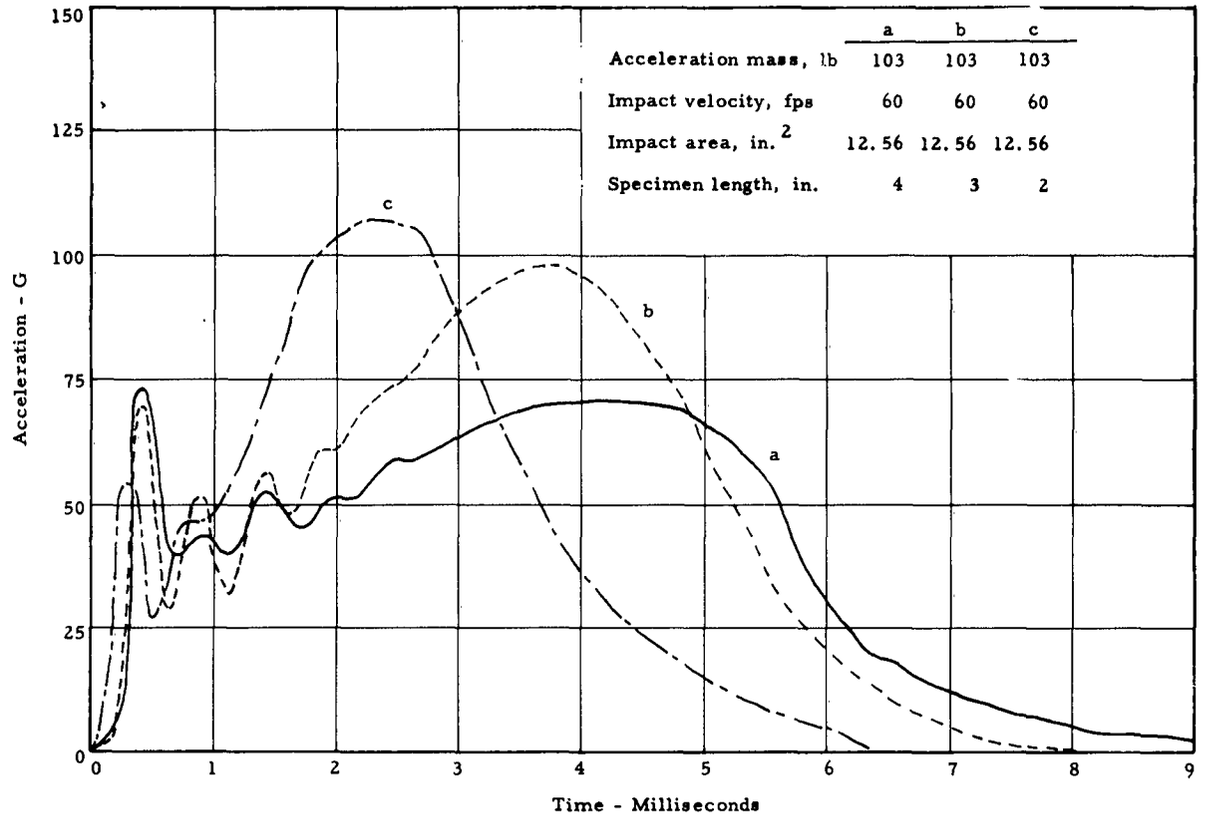

Fig. 29. Acceleration-Time Curves Showing Effect of Cushioning Thickness

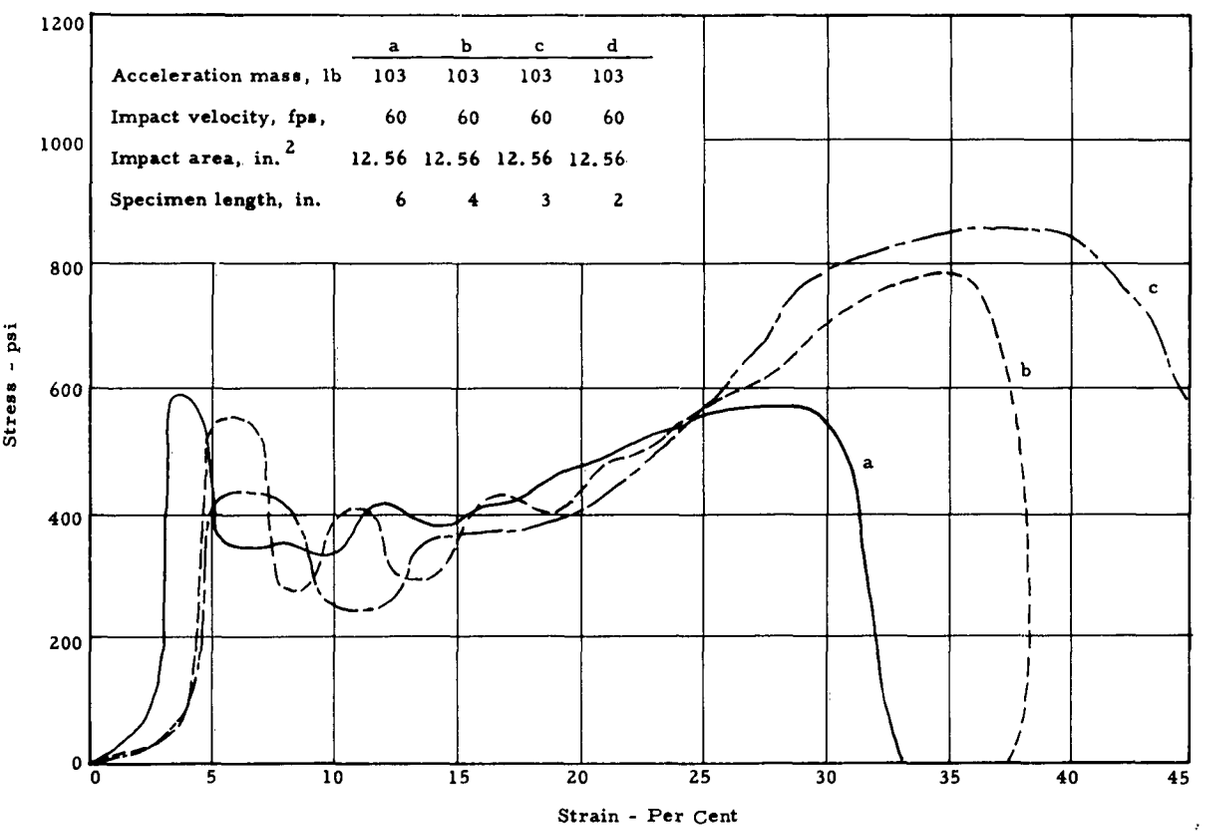

Fig. 30. Stress-Strain Curves Showing Effect of Cushioning Thickness

that the initial portions of each curve are quite similar, and the quick rise in acceleration does not occur until the material "bottoms." From this, it is apparent that when cushioning an item with a maximum allowable acceleration, it is important to use enough cushioning material so that the cushioning is not crushed beyond the strain value where "bottoming" occurs. It also shows that if a structure can stand the high acceleration, it can be protected as well with a little material having a high crushing stress as with a lot of material having a low crushing stress. However, in a structure having a low allowable acceleration, a lot of material having a low crushing stress is desirable.

It may be seen from the stress-strain curves that "bottoming" begins to occur near 35 per cent strain. This means that if, for example, a displacement of 1 ft is expected at the ground-cushioning interface in an actual installation, the total cushion thickness should be 3 ft if bottoming is to be avoided.

Shear Resistance

In these tests, it is necessary for obvious reasons to allow an appreciable clearance between the projectile and the cylinder which confines the specimen. As a consequence, the crushing of the specimen by the projectile also involves a shearing action as the projectile punches into the specimen. The shearing resistance is included in the stress-strain curves which are presented. The shear strength of this material is quite low in comparison with the compressive strength. Therefore, the effect of the shearing action on the stress-strain curves is believed to be very slight. This belief is supported by the agreement between the results presented here and those given by Covington.[2] In Covington's

measurements, the specimens were confined; but the shearing action was eliminated by using a plunger with the same diameter as the specimen. His results may have been affected somewhat by frictional resistance between the specimen and the confining cylinder. If so, the effect on the stress-strain curve is essentially the same as the effect of the shearing action referred to above.

CONCLUSIONS

All the conclusions apply to the velocity range of 24 to 120 fps.

1. The results of this investigation are essentially in agreement with those obtained with the 275-ft drop tower using the fixed force-plate-dynamometer technique.

2. Both the initial peak crushing stress and the average crushing stress of this vermiculite concrete having a damp density of about 50 lb/ft^3 (moisture content of approximately 28 per cent by volume) increase with impact velocity. For an increase in impact velocity of from 24 to 120 ft/sec, the initial peak stress increases from 570 to 650 psi, and the average crushing stress to the strain at which bottoming began increases from 310 to 550 psi. The average static crushing stress for the confined concrete is 270 psi.

3. The smallest strain at which bottoming begins is about 35 per cent. The time after impact when bottoming occurs depends on impact velocity and specimen thickness.

4. In the design of cushioning enclosures for underground structures, consideration should be given to the magnitude and rise time of the initial portion of the stress-time curve for the cushioning material.

5. The air-gun apparatus described in this report provides useful means for studying the dynamic properties of energy-absorbing materials at high impact velocities.

RECOMMENDATIONS

1. The effect of material density, moisture content, longer impact duration, higher impact velocity, and type of aggregate should be investigated.

2. A study of other types of cushioning materials such as foamed concrete, foamed plastics, foamed ceramics, and honeycomb should be made.

3. A further study of the significance of the initial peaks in the acceleration records and of methods for eliminating these peaks should be made.

APPENDIX A

CONVERSION OF ACCELERATION-TIME CURVES TO STRESS-STRAIN CURVES

Notation

The following notation is adopted for use in the equations that appear in this report

A_m = Acceleration of the cushioned mass

A_p = Acceleration of the projectile

A = Impact area of the projectile

δ_m = Displacement of the cushioned mass

δ_p = Displacement of the projectile

F_m = Resisting force of cushioning in pounds

L_o = Initial length of the cushioning material

M_m = The cushioned mass

M_p = The projectile mass

t = Time after impact

V_o = Impact velocity of the projectile

Description of Technique

Figure A-1 represents a schematic diagram of the impact of the projectile with the cushioned mass.

The acceleration of the cushioned mass during impact is recorded as a function of time. To obtain the stress-strain curve of a cushioning material for a particular impact, the following procedure is used:

Integrate twice the acceleration-time curve of the cushioned mass

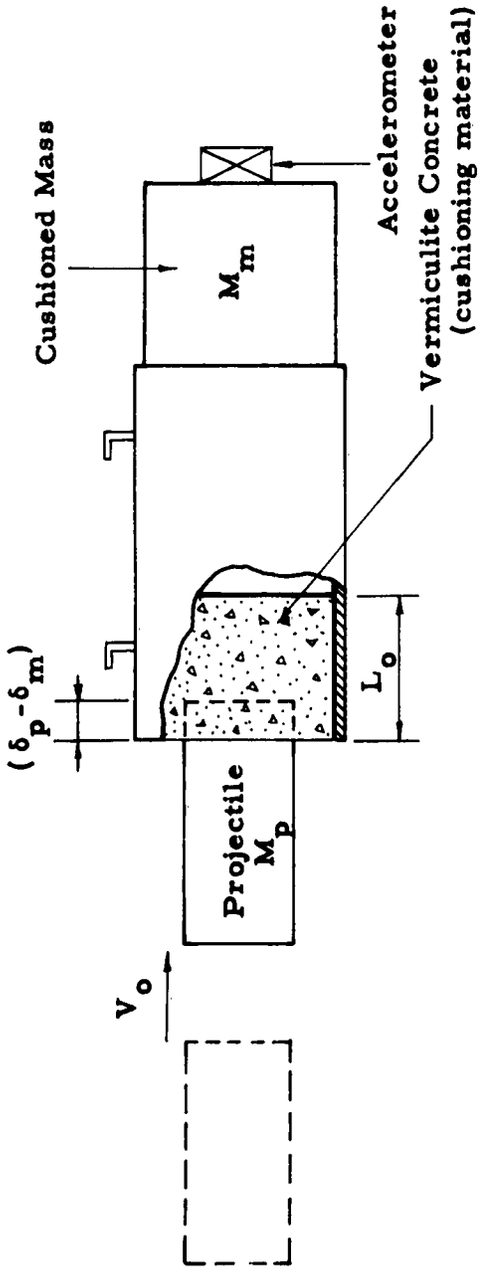

Fig. A-1. Diagram of Impact of Projectile with Cushioned Mass.

and obtain the velocity-time and displacement-time curves respectively for the cushioned mass. These integrations are represented by Eq. (A-1).

$$\int_o^t \int_o^t A_m dt\, dt = \delta_m(t) \qquad \text{- - - - - (A-1)}$$

The acceleration of the projectile is given by Eq. (A-2).

$$A_p = \frac{M_m}{M_p} A_m \qquad \text{- - - - - (A-2)}$$

The displacement of the projectile during the impact period is given by Eq. (A-3).

$$\delta_p(t) = V_o t - \int_o^t \int_o^t \frac{M_m}{M_p} A_m\, dt\, dt \qquad \text{- - - - - (A-3)}$$

The difference between the displacement of the projectile, $\delta_p(t)$, and the displacement of the cushioned mass, $\delta_m(t)$, at a specific time, t, indicates the amount of crushing of the cushioning material at time, t. Therefore, the strain in the cushioning material at time, t, is given by Eq. (A-4).

$$\frac{\delta_p - \delta_m}{L_o} = \frac{1}{L_o} \left[V_o t - \left(\frac{M_m}{M_p} + 1\right) \int_o^t \int_o^t A_m\, dt\, dt \right] \qquad \text{- - - - - (A-4)}$$

The stress in the cushioning material at the time, t, is given by Eq. (A-5).

$$F_m = M_m A_m$$

$$\sigma = \frac{F_m}{A} = \frac{M_m A_m}{A} \qquad \text{- - - - - (A-5)}$$

Eqs. (A-4) and(A-5) give all the information required for plotting the dynamic stress-strain curve.

Computer Technique

If an analog computer is available, it can be set up to do the required integrations, and to plot the stress-strain curves. This was done for the results presented in this report using the following procedure.

The original oscillograph records of the acceleration-time curves are first enlarged and replotted on 11 x 16-1/2-in. graph paper by using a Telereader with an X-Y plotter. These curves are then traced over with conducting ink so that they may be read by a curve follower which puts the acceleration-time data into the computer. The computer then does the integrating and summing required to obtain the strain, and feeds the results into an X-Y plotter. The signal from the curve follower is fed into the other axis of the plotter. Thus, as the curve follower moves along the acceleration-time curve, the stress-strain curve is drawn on the X-Y plotter.

A block diagram of the circuit used for these computations is shown in Fig. A-2. Note that the required scale factors and pot settings are also given.

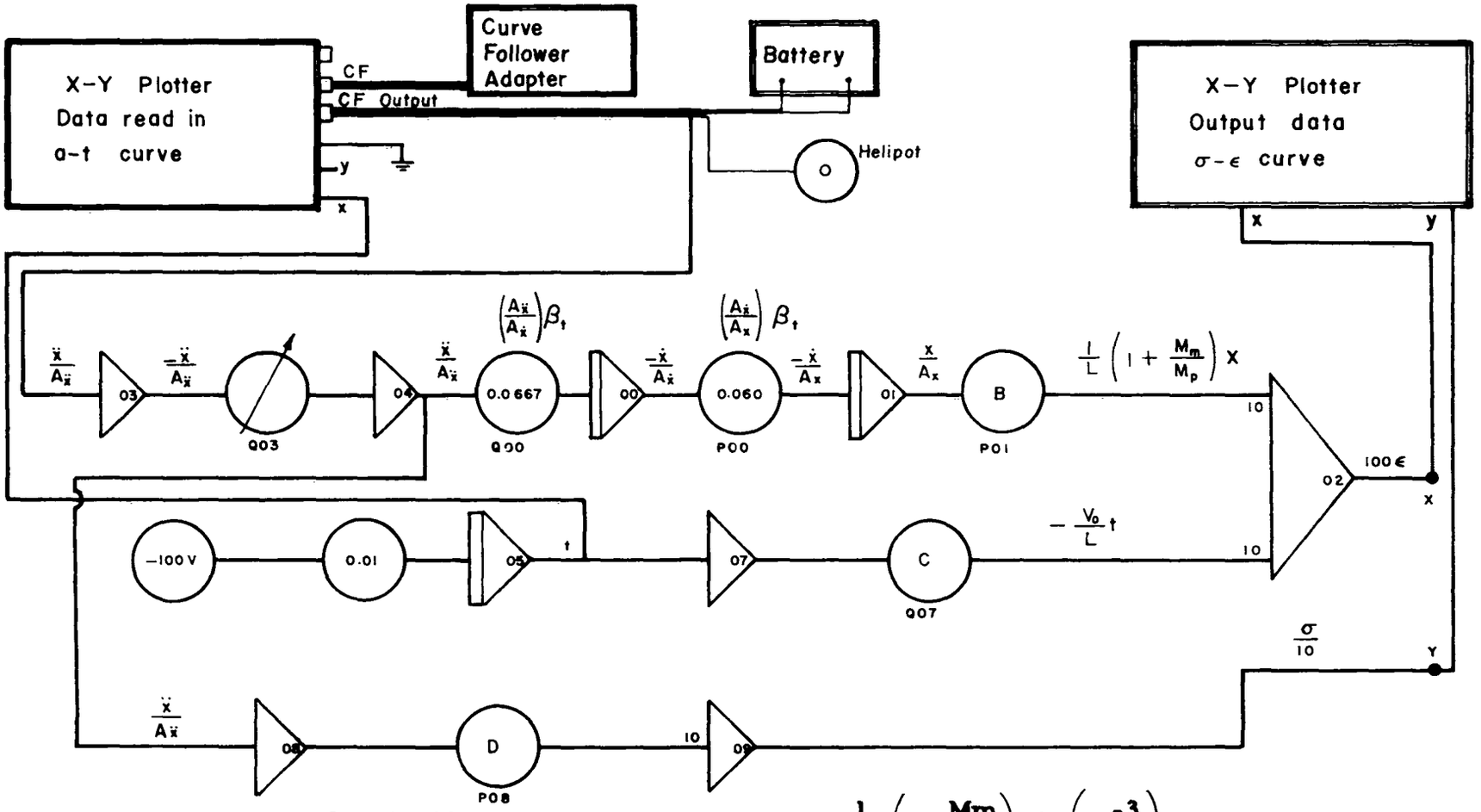

$\beta_t = 0.0001$

$A_{\ddot{x}} = 200 \frac{ft/sec^2}{v}$

$A_{\dot{x}} = 30$ ft/sec

$A_x = 5$ ft/v

$B = \frac{1}{L}\left(1 + \frac{Mm}{Mp}\right) A_x \left(10^{-3}\right)$

$C = \frac{V_o}{L}\left(10^{-3}\right)$

$D = \left(\frac{M}{A}\right) A_{\ddot{x}} \left(10^{-2}\right)$

Fig. A-2. Block Diagram of Circuit for Analog Computer Computations

APPENDIX B

THEORETICAL RESPONSE CURVE FOR ACCELEROMETER

The accelerometer used for these studies may be represented schematically as shown in Fig. B-1.

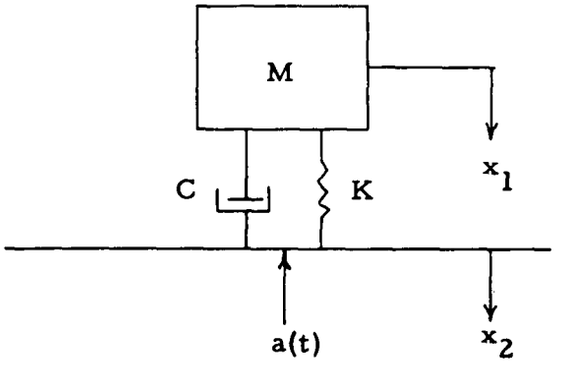

Fig. B-1. Schematic of Accelerometer Transducer

The response of this accelerometer to an input pulse a(t), shown in Fig. B-2, has been studied.

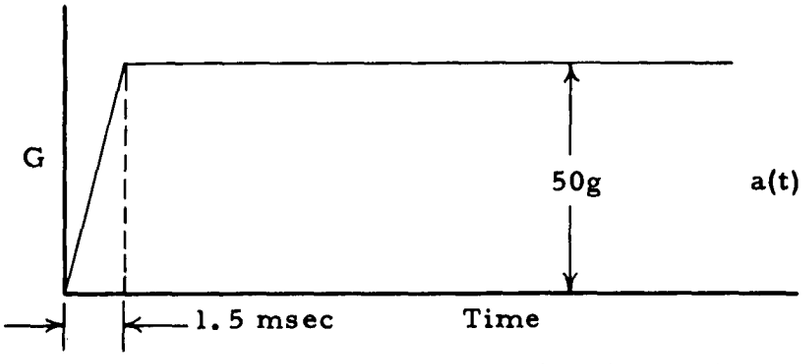

Fig. B-2. Input Pulse to Accelerometer

From Fig. B-1, it is seen that

$$x = x_1 - x_2$$
$$\dot{x} = \dot{x}_1 - \dot{x}_2$$
$$\ddot{x} = \ddot{x}_1 - \ddot{x}_2$$
$$\ddot{x} = - a(t)$$

The equation of motion of the accelerometer mass is

$$\ddot{x} + 2\zeta p\dot{x} + p^2 x = a(t) \qquad \text{- - - - - (B-1)}$$

where ζ = Damping factor (expressed as a percentage of critical)

p = Natural frequency of the accelerometer (rads/sec)

For the accelerometer investigated, the natural frequency is 2200 cps (p = 13,800 rad/sec) and ζ is approximately 0.6.

The output of the accelerometer is proportional to x with the proportionality factor being the calibration constant of the instrument.

Equation (B-1) was solved for three values of ζ with time as a variable. Results of the computations are shown in Fig. B-3. The static deflection x_{st} is the displacement of the accelerometer mass with respect to the reference plane, when the maximum acceleration has been applied for a long time. The natural period of the accelerometer is τ.

These curves indicate that for a pulse of the type studied, maximum overshoot may vary from 2 to 10 per cent depending on the damping. For the particular accelerometer used, the value of ζ is about 0.60. Hence that accelerometer can be expected to overshoot by about 6 per cent when the rise time of the acceleration pulse is about one-tenth of the natural period of the accelerometer.

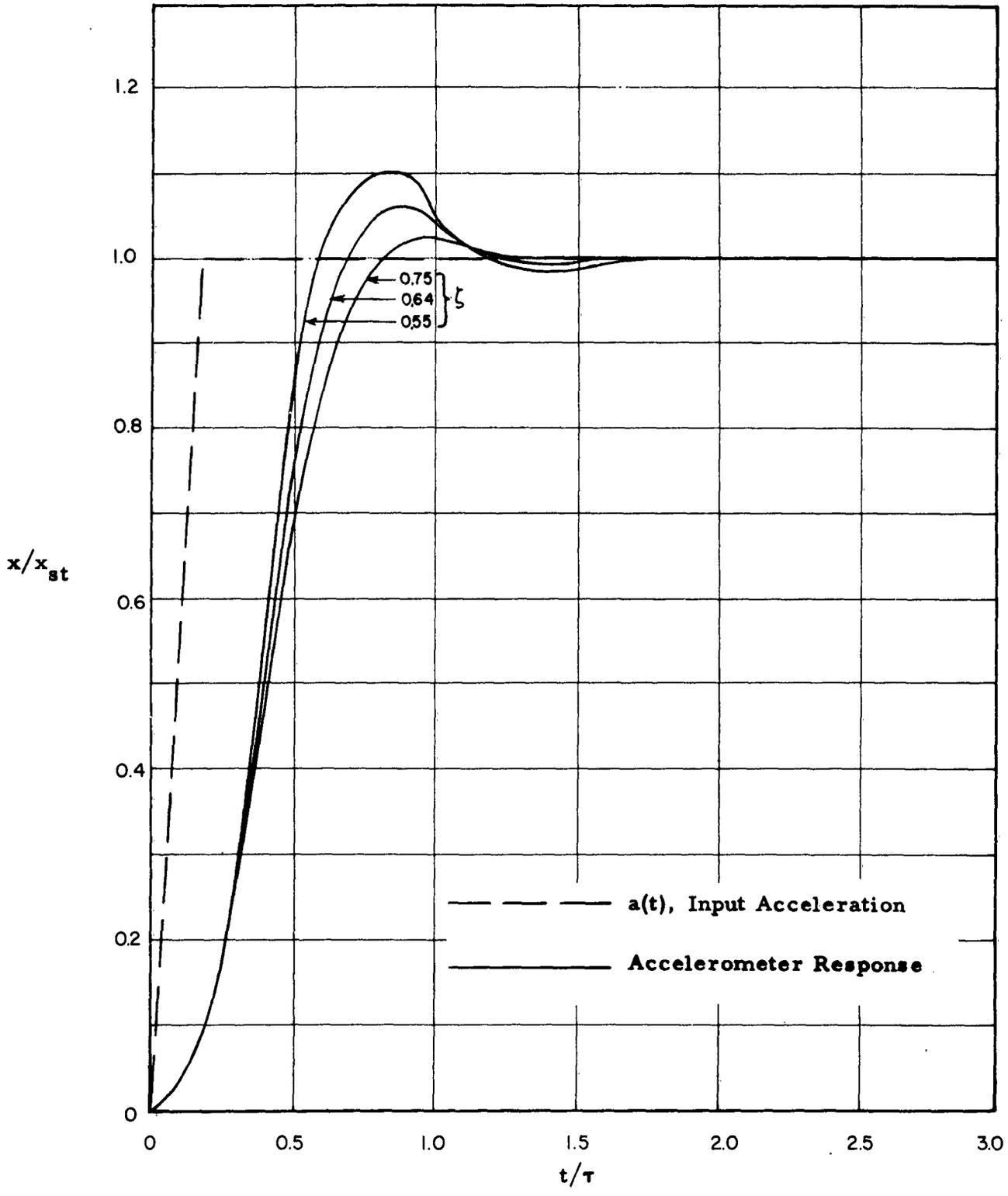

Fig. B-3. Theoretical Response Curves for an Accelerometer with a Natural Frequency of 2200 cps

BIBLIOGRAPHY

1. Vaile, R. B., Jr., Isolation of Structures from Ground Shock, Operation Plumbbob, Stanford Research Institute, Menlo Park, California, 1957.

2. Covington, C., Dynamic Energy-Absorbing Characteristics of Lightweight Vermiculite Concrete, Austin, Structural Mechanics Research Laboratory, The University of Texas, 1961.

3. Tapley, Byron D., The Effects of Shock-Induced Vibrations on Force-Sensing Apparatus, Thesis, Austin, The University of Texas, 1958.

4. Luke, Robert, R., The Impact Response of A Single-Degree-of-Freedom System With Viscous Damping, Austin, Structural Mechanics Research Laboratory, The University of Texas, 1960.

5. Richter, Albert P., Jr., The Response of a Two-Degree-of-Freedom Undamped System Subjected to Impulsive Loading, Austin, Structural Mechanics Research Laboratory, The University of Texas, 1960.

6. Huckabay, James D., A Study of the Plastic Deformation of a Single-Degree-of-Freedom System Subjected to Impulsive Loading, Austin, Structural Mechanics Research Laboratory, The University of Texas, 1960.

7. Fowler, Wallace, An Analytical Study of an Undamped Nonlinear Single-Degree-of-Freedom System Subjected to Impulsive Loading, Austin, Structural Mechanics Research Laboratory, The University of Texas, August 1961.

DISTRIBUTION LIST

ARMY

ADDRESSEE	NO. OF CYS
Chief of Engineers, DA, Washington 25, D. C., ATTN: ENGNB ATTN: ENGEB	1
Commanding General, U. S. Continental Army Command, Ft. Monroe, Va.	1
President, U. S. Army Air Defense Board, Ft. Bliss, Texas	1
Commandant, Command & General Staff College, Ft. Leavenworth, Kansas, ATTN: Archives	1
Director, Special Weapons Development, Hq CONARC, Ft. Bliss, Texas, ATTN: Chester I. Peterson	1
Commanding General, U. S. Army Chemical Corps, R&D Command, Washington 25, D. C.	1
Commanding General, Aberdeen Proving Ground, Aberdeen, Md., ATTN: Director, BRL	1
Commanding General, The Engineer Center, Ft. Belvoir, Va., ATTN: Asst Commandant, Engineer School	1
Commanding Officer, Engineer Research & Development Lab., Ft. Belvoir, Va., ATTN: Chief, Tech Support Branch	1
Commanding Officer, USA Signal R&D Lab, Ft. Monmouth, N. J., ATTN: Technical Documents Center, Evans Area	1
Commanding Officer, Chemical Warfare Lab., Army Chemical Center, Md., ATTN: Tech Library	1
Director, Waterways Experiment Station, P. O. Box 631, Vicksburg, Miss., ATTN: Library	1
The Research and Analysis Corporation, 6935 Arlington Rd., Bethesda Md., Washington 14, D. C.	1

NAVY

Director of Naval Intelligence, DN, Wash 25, D. C., ATTN: OP-922V	1
Chief, Bureau of Naval Weapons, DN, Washington 25, D. C.	2

DISTRIBUTION LIST

(Cont'd)

ADDRESSEE	NO. OF CYS
Chief, Bureau of Yards & Docks, DN, Wash 25, D. C., ATTN: D-400	1
ATTN: D-440	1
Chief of Naval Research, DN, Wash 25, D. C., ATTN: Code 811	1
Superintendent, U. S. Naval Postgraduate School, Monterey, Calif.	1
Commanding Officer, Nuclear Weapons Training Center, Atlantic, Naval Base, Norfolk 11, Va., ATTN: Nuclear Warfare Dept.	1
Commanding Officer, U.S. Naval Schools Command, U.S. Naval Station, Treasure Island, San Francisco, Calif.	1
Commanding Officer, Nuclear Weapons Training Center, Pacific, Naval Station, North Island, San Diego 35, Calif.	2
Commanding Officer, U.S. Naval Damage Control Training Center, Naval Base, Philadelphia 12, Pa., ATTN: ABC Defense Course	1
Commander, U. S. Naval Ordnance Lab., White Oak, Silver Spring, Md.	
ATTN: EA	1
ATTN: EU	1
ATTN: E	1
Commander, U. S. Naval Ordnance Test Station, China Lake, Calif.	1
Commanding Officer & Director, U.S. Naval Civil Engineering Lab., Port Hueneme, Calif., ATTN: Code L31	1
Director, U.S. Naval Research Lab., Washington 25, D. C.	1
Commanding Officer & Director, Naval Electronics Lab., San Diego 52, Calif.	
Commanding Officer, U.S. Naval Radiological Defense Laboratory, San Francisco, Calif., ATTN: Tech Info Division	1
Commander, Norfolk Naval Shipyard, Portsmouth, Va., ATTN: Underwater Explosions Research Division	1

AIR FORCE

Air Force Intelligence Center, Hq USAF, ACS/I (AFCIN-3VI), Wash 25, D. C.	1
Commander-in-Chief, Strategic Air Command, Offutt AFB, Nebraska, ATTN: OAWS	1

DISTRIBUTION LIST

(Cont'd)

ADDRESSEE	NO. OF CYS
Commander, Air Material Command, Wright-Patterson AFB, Ohio	2
Commander, Air Research & Development Command, Andrews AFB, Wash 25, D. C., ATTN: RDRWA	1
Director, Air University Library, Maxwell AFB, Alabama	2
Commander, AF Cambridge Research Center, L. G. Hanscom Field, Bedford, Mass., ATTN: CRQST-2	1
Commander, AF Special Weapons Center, Kirtland AFB, New Mexico, ATTN: Tech Info Office	1
Commandant, USAF Institute of Technology, Wright-Patterson AFB, Ohio, ATTN: MCLI-ITRIDL	1
Commander, Western Development Division (ARDC), P. O. Box 262, Inglewood, Calif.	1
Director, USAF Project RAND, Via: U.S. Air Force Liaison Office, The RAND Corporation, 1700 Main Street, Santa Monica, Calif.	1
Director of Civil Engineering, Hq USAF, Washington 25, D. C., ATTN: AFOCE	1
OTHERS	
Director of Defense Research & Engineering, Wash 25, D. C., ATTN: Tech Library	1
U. S. Documents Officer, Office of the United States National Military Representative-SHAPE, APO 55, New York, N. Y.	1
Director, Weapons Systems Evaluation Group, OSD, Room 1E880, The Pentagon, Washington 25, D. C.	1
Commandant, Armed Forces Staff College, Norfolk 11, Va., ATTN: Library	1
Commander, Field Command, DASA, Sandia Base, Albuquerque, New Mexico	5
Commander, Field Command, DASA, Sandia Base, Albuquerque, New Mexico, ATTN: Training Division	2
Chief, Defense Atomic Support Agency, Washington 25, D. C.	5

DISTRIBUTION LIST

(Cont'd)

ADDRESSEE	NO. OF CYS
Chief, Defense Atomic Support Agency, Washington 25, D.C., ATTN: Major Vickery	2
Commandant, Army War College, Carlisle Barracks, Pa., ATTN: Library	1
Commandant, National War College, Washington 25, D. C., ATTN: Class Rec Library	1
Commandant, The Industrial College of the Armed Forces, Ft. McNair, Washington 25, D. C.	1
Officer-in-Charge, US Naval School, Civil Engineering Corps Officers, US Naval Construction Battalion, Port Hueneme, Calif.	1
Los Alamos Scientific Laboratory, P. O. Box 1663, Los Alamos, New Mexico, ATTN: Report Librarian (For Dr. Alvin C. Graves)	1
Administrator, National Aeronautics & Space Administration, 1512 "H" Street N.W., Washington 25, D. C.	1
Langley Research Center, NASA, Langley Field, Hampton, Va., ATTN: Mr. John Stack	1
Chief, Classified Technical Library, Technical Information Service, U. S. Atomic Energy Commission, Washington 25, D.C., ATTN: Mrs. Jean O'Leary	1
Manager, Albuquerque Operations Office, U. S. Atomic Energy Commission, P. O. Box 5400, Albuquerque, New Mexico	1
Dr. Robert J. Hansen, Division of Industrial Cooperation, Massachusetts Institute of Technology, 77 Massachusetts Ave., Cambridge, Mass.,	1
Dr. Bruce G. Johnston, The University of Michigan, University Research Security Office, Lobby 1, East Engineering Bldg, Ann Arbor, Michigan	1
Sandia Corporation, Sandia Base, Albuquerque, New Mexico, ATTN: Classified Document Division (For M. L. Merritt)	1
Superintendent, Eastern Experiment Station, U. S. Bureau of Mines, College Park, Md., ATTN: Dr. Leonard Obert	1
Dr. Nathan M. Newmark, University of Illinois, Room 207, Talbot Lab., Urbana, Illinois	1
Commander, ASTIA, Arlington Hall Station, Arlington 12, Va., ATTN: TIPDR	20

DISTRIBUTION LIST

(Cont'd)

ADDRESSEE	NO. OF CYS
Holmes & Narver Inc., AEC Facilities Division, 849 S. Broadway, Los Angeles 14, Calif., ATTN: Mr. Frank C. Galbright	1
American Machine and Foundry, 7501 North Natchez Avenue, Niles, Illinois	1
Southwest Research Institute, 8500 Culebra Road, San Antonio 6, Texas	1
Armour Research Foundation, 10 West 35th Street, Chicago 16, Illinois	1
Barry Wright Corporation, 700 Pleasant Street, Watertown 72, Massachusetts	1
Roland F. Beers, Inc., P. O. Box 23, Alexandria, Virginia ATTN: Mr. Sherwood B. Smith	1
Iowa State University, Ames, Iowa	1
NESCO, 711 South Fair Oaks Avenue, Pasadena, California	1
Engineering-Physics Company, 5515 Randolph Road, Rockville, Maryland	1